Atomic layer deposition of thin films containing alkali metals

Series of dissertations submitted to the
Faculty of Mathematics and Natural Sciences, University of Oslo
No. 1479

ISSN 1501-7710

Cover: Inger Sandved Anfinsen.
Printed in Norway: AIT Oslo AS.

Produced in co-operation with Akademika Publishing.
The thesis is produced by Akademika Publishing merely in connection with the thesis defence. Kindly direct all inquiries regarding the thesis to the copyright holder or the unit which grants the doctorate.

Preface

This thesis is submitted in partial fulfilment of the requirements for the degree of Ph.D at the Department of Chemistry and Centre for Materials Science and Nanotechnology, Faculty of Mathematics and Natural Sciences, University of Oslo. The experimental work is carried out at the NAFUMA (Nano- and Functional Materials) group under the supervision of Prof. Helmer Fjellvåg and Ass. Prof. Ola Nilsen between September 2009 and December 2013.

After spending six years at the NAFUMA-group there are many people to thank, many which have contributed in their own way to make my stay here interesting and rewarding. I would first thank my supervisors for accepting me as their student, without them, there would be no thesis. I will also acknowledge the opportunities I got to do advanced experiments at large facilities, it has been something that has opened my eyes and I have learned a lot.

My thanks go to the ALD- and battery-groups, it has been very interesting to work and collaborate with all of you. I must also thank all of my colleagues who have also been my friends, especially; Madeleine, Mari, Laurent, Christoph, Hiroshi, Per-Anders, Knut, Kristin, Karina, Chris and Dave, it has been fun to work with you all. Thanks to Ville for telling me about Finland, and thanks to Atle for inviting me to collaborate on his projects. And lastly, I must especially thank both my office-mate through many years, Jon, and my trusted co-author Henrik for all the interesting discussions we have had and the fun we have had afterwards.

I must thank my family and friends outside the University, for the support and patience I have got through the years of studies. And finally, big thanks goes to Monika for always being loving and supportive.

Abstract

This thesis presents experimental work on thin films of different compounds containing lithium, sodium or potassium has been synthesized by atomic layer deposition (ALD). The overall motivation for this work has been to develop materials and methods to improve lithium ion battery technology by using ALD.

A cathode in a lithium ion battery should have a long operating life, be environmentally benign and have high capacity and power density. Vanadium oxides are popular as cathodes in lithium ion batteries due to their relative low price and potentially high capacity. Most studies of vanadium oxide cathodes shows relatively short lifetime of the cathode or relatively fast cathodes. In this work a high power thin film cathode of V_2O_5 for lithium ion batteries has been developed. The cathode is deposited by ALD using $VO(thd)_2$ and ozone, which displays a rather peculiar type of ALD-growth. This peculiar growth is studied in detail, and the optical properties of these films are investigated. The films have an unusually rough surface, and it was found that a 10nm thick film deposited at 235^{o}C consisted of individual nano particles. The 10 nm thick cathode has been shown to endure more than 4000 discharge-cycles at 120C and almost 1600 cycles while staying within 80% of the original capacity. The same cathode was also shown to sustain discharge rates of 960C which corresponds to a discharge in 3.75s. The power density obtained in this work bridges the gap between super capacitors and batteries and the combination of long lifetime and high discharge rate is not found previously for thin film batteries of V_2O_5.

ALD of lithium containing materials has attracted widespread interest the last few years. The number of known precursors for lithium has grown, but the complete picture is still not understood. Therefore lithium hexamethyldisilazane (LiHMDS) is explored as a precursor for ALD of lithium compounds. The precursor is shown successful in deposition of Li_3N, Li_2CO_3 and $LiNbO_3$. The deposition of Li_3N may be an important step to deposit solid electrolytes and the deposition of Li_2CO_3 proved to be important for proving the growth of oxides using this precursor. When comparing the growth of Li_3N and Li_2CO_3 it was found significant difference in the surface chemistry. The $LiNbO_3$-films were shown to be ferroelectric with an unusually high coercive field. It proved possible to deposit epitaxial $LiNbO_3$ on single crystal substrates of $LaAlO_3$ and Al_2O_3 and the orientation of the films could be controlled by the orientation of the substrate.

A milestone in atomic layer deposition of lithium compounds would be to deposit a full battery. In order to realize this, a lithiated cathode material must be deposited. The cathode material $LiMn_2O_4$ was also studied in this work. It was discovered that the amount of lithium in the deposited films is more or less independent of the number lithium cycles to manganese cycles. It is hypothesized that the ligand of the lithium precursor reduces the manganese and the lithium is intercalated into the manganese oxide. This is a new approach to ALD of lithium compounds and the term film body controlled lithium deposition is used to describe the mechanism. The use of LiHMDS is also attempted in deposition of $LiMn_2O_4$, with no success.

Sodium and potassium are among the few elements in the periodic table which are not yet used in ALD. Sodium and potassium are relatively similar to lithium and exploring the deposition of these elements will hopefully shed new light on the deposition of lithium compounds. Many oxides of sodium and potassium also have piezo- and ferroelectric properties, and the sodium ion battery is predicted to be a way to combat lithium shortage. Atomic layer deposition of sodium and potassium oxides is reported for the first time in this thesis. Six different precursors are investigated and evaluated and precursors for sodium and potassium. The initial study was performed by depositing sodium and potassium aluminates, in order to evaluate the precursors. The process for the aluminates was found to scale up to the 200mm wafer scale. The precursors were found to work in a large temperature window and react with both water and ozone, thus proving to relatively flexible and possible to combine with most known ALD-processes. Further development into deposition of sodium based ferroelectrics then explored by deposition of sodium tantalate and sodium niobate.

Contents

Glossary

ALD	Atomic layer deposition
C	Discharge rate in discharges per hour
CMOS	Complementary metal–oxide–semiconductor
CV	Cyclic voltammetry
CVD	Chemical vapour deposition
EtCp	1-ethyl-cyclopentadienyl ($C_5H_4C_2H_5^-$)
FeRAM	Ferroelectric random access memory
HF	Hydrogen fluoride (HF)
HMDS	Hexamethyldisilazane ($N(Si(CH_3)_3)_2^-$)
IR	Infrared
LED	Light emitting diode
MEMS	Microelectromechanical system
OEt	Ethoxy/ethoxide ($C_2H_5O^-$)
OtBu	tert-butoxy/tert-butoxide ($C_4H_9O^-$)
PLD	Pulsed laser deposition
SE	Spectroscopic ellipsometry
SEI	Surface electrolyte interface
thd	2,2,6,6-tetramethyl-hepta3-5-dionate
TMA	Trimethyl aluminium ($Al(CH_3)_3$)
TMPO	Trimethyl phosphate ($(CH_3)_3PO_4$)
TMSO	Trimethyl silanolate ($OSi(CH_3)_3^-$)
UV-VIS	Ultra violet - visible spectroscopy

List of papers

I. Optical properties of vanadium pentoxide deposited by ALD
Erik Østreng, Ola Nilsen, Helmer Fjellvåg. *J. Phys. Chem. C,* **2012** 116(36), 19444-19450.

II. Ultrafast V_2O_5 cathodes for thin film micro batteries by ALD
Erik Østreng, Knut B. Gandrud, Ola Nilsen, Helmer Fjellvåg. *J. Mater. Chem. A.* **Submitted**

III. Atomic layer deposition of lithium nitride and carbonate using lithium silylamide
Erik Østreng, Ponniah Vajeeston, Ola Nilsen, Helmer Fjellvåg. *RSC Advances*, 2(15), **2012**, 6315-6322

IV. Atomic layer deposition of ferroelectric $LiNbO_3$
Erik Østreng, Henrik H. Sønsteby, Ola Nilsen, Helmer Fjellvåg. *J. Mater. Chem. C*, **2013,** 1, 4283-4290

V. Atomic Layer Deposition of Spinel Lithium Manganese Oxide for Thin Film Lithium Ion Batteries
Ville Miikkulainen, Amund Ruud, Erik Østreng, Ola Nilsen, Helmer Fjellvåg. *J. Phys. Chem. C*, **2013,** DOI: 10.1021/jp409399y

VI. Atomic layer deposition of Sodium and Potassium oxides: Evaluation of precursors and deposition of thin films
Erik Østreng, Henrik H. Sønsteby, Sigurd Øien, Ola Nilsen, Helmer Fjellvåg. *In preparation*

VII. Epitaxial perovskites of sodium and potassium niobates by ALD
Henrik H. Sønsteby, Erik Østreng, Ola Nilsen, Helmer Fjellvåg. *In preparation*

In addition, I have contributed to the following papers:

VIII. Atomic layer deposition of functional films for Li-ion microbatteries
Ola Nilsen, Ville Miikkulainen, Knut B. Gandrud, Erik Østreng, Amund Ruud, Helmer Fjellvåg. *Physica Status Solidi A*, DOI: 10.1002/pssa.201330130

IX. Deposition and x-ray characterization of epitaxial thin films of $LaAlO_3$
Henrik H. Sønsteby, Erik Østreng, Ola Nilsen, Helmer Fjellvåg. *Thin Solid Films,* **2013,** 550, 90-94

X. Atomic Layer Deposition of $LaPO_4$ and Ca:$LaPO_4$

Henrik H. Sønsteby, Erik Østreng, Ola Nilsen, Helmer Fjellvåg. *Chemical Vapor Deposition* ,**Submitted**

1 Introduction

State of the art functional materials are often so important for society that they define the name of the age, such as the Stone Age or the Iron Age. What our age will be named is hard to predict, but it is certain that our progress and standard of living is strongly dependent on our materials. Every day we use and take for granted a large variety of materials of different sizes and scales. Everything from construction materials as steel, glass, concrete and plastics to electrical conductors such as copper are an integral part of our lives. We also rely heavily on materials with advanced functional properties in our modern society. Materials such as semiconductors, catalysts, insulators, magnetic materials or materials for energy storage and production are important for our technology and devices. Increasing material performance and development of new materials is what drove humans out of the caves and into skyscrapers and replaced the stone axe with a smart-phone. Materials are not only the core of our technology, but also of our art and our culture.

Energy consumption is a defining property of a civilisation; it is a measure of productivity and a measure of living standard. Many functional materials are in some way connected to how we are harvesting, transporting or utilizing energy, such as electroactive materials in batteries and fuel cells, catalysts for production of chemicals or semiconductors in solar cells and computers to name a few. We cannot meet our energy demands without construction materials or functional materials as the devices and machinery that consumes the energy are also made from materials of some sort. In the last few decades, energy distribution and storage has also become dependent on functional materials in the form of batteries or in the form of hydrogen storage. Energy storage is of paramount importance when utilizing energy from renewable sources, as the supply and demand for wind and solar energy are rarely in phase. Electrochemical storage of energy relies on many different types of materials which should function together at a variety of conditions. In fuel cells and batteries the materials are exposed to large chemical- and electrical potential gradients, high current densities and ions which move through solid materials and interfaces as well as to phase transitions during operation, which are quite brutal conditions. In order to cope with these conditions materials need to be designed on many different scales. In materials science it is not just the chemical composition that is important for the function but also crystalline structure, texture and morphology of the material. With the advent of nano-science it has become clear that also the

shape and size can define the properties of materials and by working on all these scales we can design materials with a new degree of freedom.

As devices are becoming smaller and more mobile, integration of the energy supply into the device is increasingly important. Micro batteries are of increasing importance for development of among other things medical-, communication- and entertainment-technologies. The technological development the past decades have given us computers and other devices with increasing speed and storage, but recently there has been a shift where mobility and size has become an important parameter. This trend does not only apply to computers and cell phones, but also to devices such as medical devices, motion sensors and communication tags. The demand for mobility also calls for increasingly advanced batteries, and the possibility to integrate batteries into the device.

Another important dimension to technological development is to use environmentally benign materials. The history of technology is full of examples such as leaded fuels, acid rain and climate change where the cost of progress has been higher than expected. Therefore a range of materials such as lead are banned from use. In battery production the uses of metals such as lead and cadmium are problematic and should therefore be substituted. In this thesis a cathode for lithium ion batteries made from V_2O_5 have been developed and the performance and lifetime have been shown to be superior to most other reported V_2O_5-based cathodes in the literature. Lead based ferroelectrics are known for their high performance, but due to environmental concerns new lead-free ferroelectrics should be developed. In this thesis new ALD-processes for the alkali metals are developed with the aim of producing new piezo- and ferroelectric materials. The niobates and tantalates of the alkali metals are deposited and studied and $LiNbO_3$ is studied extensively and found to be ferroelectric.

Atomic layer deposition (ALD) is a method for producing thin films with very high precision. Films produced using this technique can be controlled down to a fraction of a nanometre with extremely good uniformity and reproducibility. ALD can also be utilized for deposition on surfaces with 3D structures. The uniformity and the indifference to substrate morphology enable the use of ALD in most areas of nanotechnology and research. ALD has over the last 40 years been used to deposit a wide host of materials, with an equally wide range of applications. Methods for depositing compounds of most of the elements in the periodic table

have been developed during the history of ALD. However, it is only in the recent years that processes for lithium compounds have reported. In this thesis the first results for deposition of sodium and potassium oxides are reported.

2 Applications of alkali metal compounds

This chapter will outline some applications of alkali metal compounds, especially in battery technology and give an introduction to dielectric materials.

2.1 Batteries

Every new generation of consumer technology is required to have better performance, be less expensive and more efficient. This seems like an impossible task, but by developing better materials, making the constituent parts smaller and more efficient and scaling the production, it has proven possible for several decades. For a mobile device, improved performance ideally includes a better battery. Unfortunately, the capacity of a battery is limited by chemistry and hence the capacity cannot be increased at the same rate as semiconductor technology. However, making a better battery does not necessarily mean only higher capacity, but can also mean for instance increased stability, charge rate or voltage. These properties are not only dependant on the elemental content and can often be improved by nano structuring.

A battery is in principle, a simple device and it consists of three main parts which are common to all types and designs of batteries: a cathode, an electrolyte and an anode. Depending on the design the components and chemistry will be different, but the operating principle is always that the electrolyte transports some ion from the anode to the cathode while at the same time an electron is transferred in an outer circuit, as outlined in Figure 1. This effectively causes an oxidation to occur at the anode while the cathode is reduced. As this work is concentrated on alkali metals, batteries using these metals will be used as examples here.

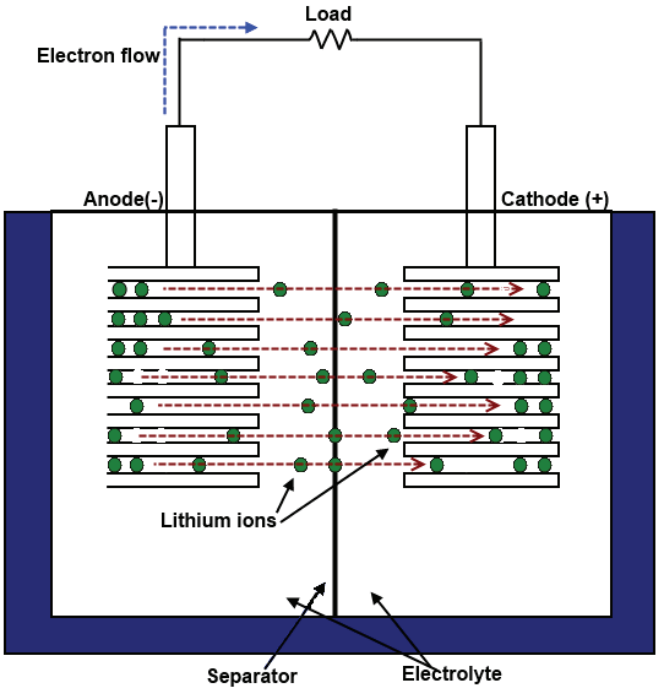

Figure 1 Illustration of the parts and operation of a lithium ion battery during discharge. The lithium ions move from the anode to the cathode, which are separated by a separator and an electrolyte while the electrons drive the load.

Lithium and sodium ion batteries

A lithium ion battery is a secondary battery where lithium ions are moved from the anode to the cathode during discharge. Lithium has the most negative standard reduction potential of the elements in the periodic table. Considering that lithium is also the lightest metal both in terms of molar mass and density; both the energy- and power-density of lithium ion batteries are high. The lithium ion battery does not have the disadvantages which lead-acid, nickel-cadmium or nickel-metal hydride has such as the high weight and hydrogen production during charge. Lithium ion batteries on the other hand are expensive and also have some safety issues. Commercial batteries which have flammable electrolytes in the form of an organic solvent have caused accidents and fires [1, 2].

A lithium ion battery consists of the same three parts as all batteries - cathode, anode and electrolyte. The materials for these components are required to be good lithium ion

conductors, or be nano structured in such a way that the diffusion distance through the electrolyte is very short. The electrodes are also required to be electronically conductive, which enables the transport of electrons from the current collector to where the lithium ions are to be intercalated. The electrolyte on the other hand is required to be an electrical insulator; otherwise the battery would self-discharge rapidly.

The anode could be made from metallic lithium which gives the highest voltage and capacity per weight or volume. However, lithium anodes are prone to some disadvantages, especially safety issues and dendritic growth of lithium on the anode during charging which eventually short circuits the battery [3]. The anode is therefore often lithium ions intercalated into carbon [4], metal oxides [5], nitrides [6] or metals such as tin [7]. Silicon is also suggested as a high capacity anode – but the volume work is too large for a long lifetime of the assembled batteries [7, 8]. The mentioned anodes have capacities in the range 300 mAh/g to 3900 mAh/g for graphite and metallic lithium, respectively and the oxide and nitride anodes between 400-1000 mAh/g. The voltages vs. Li/Li^+ of these materials range from ~1.5 V for the oxides to 0.7V for the nitrides and 0.05-0.2V for the carbons [3]. The high capacities suggest that the main contribution to increased capacity per weight or volume does not come from improving the anode, but rather the cathode.

Cathodes for lithium ion battery should also ideally consist of materials with high electronic and ionic conductivity, and react with lithium in a reversible way. One of the first breakthroughs in cathode materials were TiS_2 [9], which is a layered compound. Layered compounds are materials which have crystal structures which are built up from sheets. The sheets separated by ions and these structures have the advantage that they often allow for high ion mobility in the space between the sheets. Later, layered oxides, such as $LiMO_2$ (M=Ni, Co, Mn) were discovered to have higher intercalation potential than the sulphides and the first commercial lithium ion battery, marketed by Sony, utilized layered $LiCoO_2$[10]. In the last two decades, other structure classes such as the manganese oxide spinels [11] and the $LiFePO_4$ [12] have also been commercialized. These common cathode materials have capacities from about 140 mAh/g for $LiCoO_2$ to about 220 mAh/g for the vanadium oxides, and the other mentioned materials, between 160-180 mAh/g [3]. A limitation of the cathode materials most commonly used in commercial applications, such as $LiFePO_4$, $LiCoO_2$ of $LiMn_2O_4$ is that they exchange at most one electron per transition metal ion, and often less. A

big paradigm shift would therefore be to increase the number of electrons exchanged as this would literally double the capacity of the battery without increasing the mass or volume [3]. Exchanging more electrons often causes different voltages during discharge and often the intermediate phases have different conductivities and are unstable, causing precipitation of electrochemically inactive phases. Elements such as tungsten and molybdenum can form compounds which can exchange more than one electron per formula unit. However, molybdenum and tungsten are quite heavy and do not necessarily contribute to net gain in specific capacity. An alternative is vanadium, which can form oxides that exchange more than one electron, but the life time is short and the kinetics is slow when exchanging more than one electron per vanadium atom from V_2O_5.

The demand for high intrinsic conductivities is not absolute. For instance $LiFePO_4$ is a quite poor electronic and ionic conductor, but still a successful cathode material when prepared as nano particles [10]. There are also other advantages to nano structuring of electrodes, such as increased rate capability and longer lifetime[8]. The increased lifetime gained from nano structuring originates in the ability of smaller particles to cope with the volume variations of repeated lithium insertions [13].

Electrolytes for lithium ion batteries should have high mobility of lithium and high electronic resistivity, allowing them to only transport lithium ions between the electrodes and no electrons. Electrolytes can be divided into two main categories, solid and liquid. Liquid electrolytes are normally used in commercial batteries and consists of a lithium salt in an organic solvent [14] or an ionic liquid which contains lithium [15, 16]. The liquid electrolytes have the advantage that they are inexpensive and easy to prepare. On the other hand, they are also a safety concern due to the flammable solvents used [17, 18] and the toxic products such as HF are released if the electrolyte salts comes in contact with water. Another drawback with liquid electrolytes is the decomposition of the solvent when charged at high voltages, which limits the potential to about 4V for lithium ion batteries with liquid electrolytes. All these problems can be potentially be circumvented with the application of a solid - polymeric, ceramic or glassy – electrolyte, which does not suffer from decomposition at high voltages [16, 18-20]. These electrolytes can be materials such as LiPON, amorphous $LiTaO_3$, lithium phosphide sulphide glasses or complex oxides such as lithium lanthanum titanate or -zirconate [16, 21-24]. The conductivities of solid electrolytes at room temperature are typically between

~10^{-3} and ~10^{-8} S/cm [16, 22, 24], compared to ~10^{-3}S/cm for liquid electrolytes [14]. Low conductivities could be compensated by a thinner electrolyte or higher operation temperature. Yet, the implementation of solid electrolytes is not simple, especially due to the chemical compatibility between the electrodes and electrolytes during sintering [16] and mechanical properties of the electrolyte [22] .

Na-ion batteries

A similar type of battery as the lithium ion battery is the sodium ion battery. The basic design and construction is similar, however the sodium ion battery is not yet commercialized to the same degree as the lithium ion battery. The sodium ion battery has a few obvious advantages, primarily the amount of sodium in the world which is about 1000 times higher than the amount of lithium. Sodium is also readily available from seawater and sodium chloride could be mined, making the sodium available everywhere on the planet. In contrast, the amount of lithium in the world is projected to be a problem if electric vehicles should be fitted with lithium ion batteries. However, it is debated if the lithium supplies actually will run out[15]. Another advantage of sodium batteries is that the cathodes could readily be made from oxides of common metals such as iron, vanadium and manganese.

Although sodium ion batteries have some advantages, they also have some disadvantages compared to lithium ion batteries. The disadvantages arise mostly from the properties of sodium. Sodium have higher molar mass which will cause lower capacity, while the lower reduction potential causes lower cell voltages and a larger ionic radius which gives slower diffusion and kinetics [25]. Lastly, the low melting point of 98 ^{o}C can be a potential safety issue [25]. Thus at the moment the sodium ion battery is a supplement to lithium ion batteries for larger applications such as stationary energy storage and electric vehicles.

The sodium ion battery research field is not as mature as the lithium field, and such there is big room for improvement of the materials. Pure solid sodium anodes cannot be used with liquid electrolytes in commercial batteries for safety reasons as the dendrite formation is even more prominent for sodium compared to that for lithium. The anodes for first generation sodium ion batteries are thought to be carbons, which have a capacity of about 220 mAh/g [25]. Cathode materials which are investigated are either oxides which are analogous to the layered or spinel oxides used in lithium ion batteries or novel compounds such as the

fluorophosphates [26]. The liquid electrolytes used are currently also analogues of the lithium electrolytes. However a recent review [25] indicates that organic solvents corrode the anodes and does not form the stable surface-electrolyte-interface (SEI), which is formed in lithium ion batteries. This suggests that integration of solid electrolytes could make a big impact on sodium ion batteries as there already exist good solid state sodium ion conductors, such as the β-alumina [27].

Thin film batteries

A battery does not necessarily have to be assembled from powders and liquid electrolytes; it could also be made from a stack of thin films. A thin film battery will obviously contain less electroactive material than a bulk battery, and hence the total capacity of a thin film battery will be low. However this is not necessarily problematic in the applications areas of thin film batteries. Such batteries are thought to have applications in technologies such as CMOS and MEMS, medical implants or smart cards [23, 28, 29] where the power consumption is low. A thin film battery has some advantages compared to a normal battery, such as shorter diffusion paths and the potential for much faster discharge rates than a normal battery. For a thin film battery there is no need for binders and carbon which yield higher efficiencies [23] and longer lifetime [29]. It is very desirable to utilize solid state electrolytes in thin film batteries. A solid electrolyte can be prepared with a thickness of < 1μm, compared to liquid electrolytes which are normally in the range of 20μm [30].

Thin film batteries have previously been prepared using techniques such as PLD [28] sputtering [31]. However, deposition of thin films of only the cathode materials without the rest of the battery structure using CVD has also been proven for $LiCoO_2$ [32, 33] and V_2O_5 [34-36]. PLD and sputtering have been utilized to successfully deposit batteries on flat substrates with performances close to the theoretical capacity and with very long life time [23, 28, 31]. Notten *et al.* have pointed out that these systems do not necessarily provide sufficient energy for the desired applications [29]. Their proposed solution was to increase the surface area of the battery without increasing the footprint by making a *"3D-integrated all-solid-state battery"*. This concept, which has not yet been realized, estimates energy densities of about 5 $mWh/\mu m \cdot cm^2$ compared to 0.1 $mWh/\mu m \cdot cm^2$ [29, 37], *i.e.* a 50-fold increase compared to planar thin film battery structures. A key to realize such a concept is the ability to deposit thin films on a 3D structured substrate. ALD is the only known thin film technique which can

deposit thin films of complex oxides on the high aspect ratio substrates, which are needed as templates for this type of battery [29].

There are already commercial all solid state thin film batteries on the market [38-40] built for integration in devices. These devices are specified to endure more than a decade of service and 100'000 discharge cycles [38], due to the use of solid electrolytes. The dimensions of the smallest packaged commercial batteries are in the order of 5 x 5 x 1 mm^3. The thickness is quite large, however, the active battery structure can be as thin as 10-20µm and the bulk of the thickness comes from packaging to protect the battery from air and moisture [41]. Commercial batteries can be deposited either on silicon [39] or on polymer substrates using either PECVD or sputtering of $LiCoO_2$, V_2O_5 or $LiMn_2O_4$ as cathode materials and tin-based anodes [40]. The commercial alternative to thin film batteries are supercapacitors [42], however the thin film batteries are already superior to supercapacitors in terms of voltage and energy density, while the supercapacitors are superior in terms of power density. Commercial batteries can also be supplemented with energy harvesting modules for full wireless operation [38, 39]. The prices for such batteries are below $0.5 for a 4V, 50µAh battery [39].

2.2 Electrical properties of alkali metal oxides

Alkali metal oxides can have other functional properties than electrochemical properties. The perovskite related complex oxides of the alkali metals and a six-valent metal are insulators and often piezo- or ferroelectric, depending on composition and temperature. Apart from insulators, $Na_xCoO_2 \cdot yH_2O$ is also known to be superconductor [43] and Na_xCoO_2 is known to be a thermoelectric[44, 45].

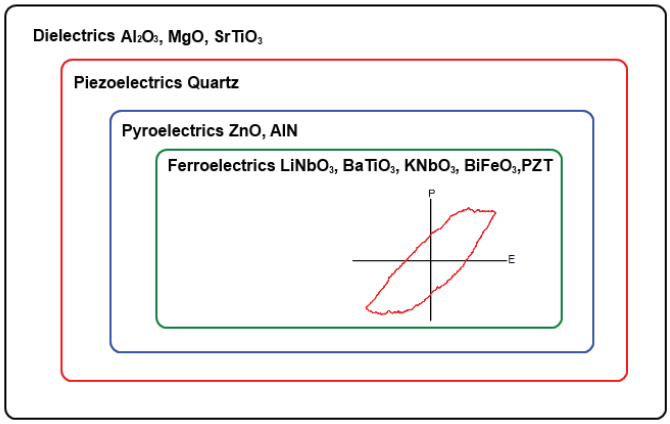

Figure 2 Comparison of different classes of dielectric materials with examples of materials.

Figure 2 shows an overview of different classes of dielectric materials with some examples. The figure illustrates that all ferroelectrics must be pyro-, piezo- and dielectric, but only some of the dielectric materials are piezo-, pyro- and/or ferroelectrics. This classification has, of course, some physical origin which can be traced back to the placement of atoms inside the material and can be explained by the symmetry of the crystal. A piezoelectric material must be both insulating and have a point group without a centre of symmetry in its crystal structure, the exception is the point group 432 which cannot be piezoelectric. If the material also has a unique polar axis, which causes a permanent polarization in the material, it is pyro electric. The lack of centre of symmetry allows for a relative displacement of the centre of gravity of positive and negative ions in the structure. The shift can be induced by mechanical stress, in the case of piezoelectrics and thermal gradients, in the case of pyroelectrics. The reverse will also be true; mechanical deformation of the material or temperature change under the application of an electric field. The applications of piezoelectrics are many, but especially electromechanical systems such as motors and actuators[46], and pressure sensors are a prime uses of piezoelectrics in modern technology. Pyroelectrics have found use in infrared sensors, where the performance is comparable to that of semiconductor diodes, without the need for cooling required for diode detectors [46, 47].

Ferroelectrics are pyroelectrics which can have a spontaneous polarization in two different directions. Ferroelectrics are characterized by hysteresis behaviour of the polarization upon the applied field which originates from the two different directions of spontaneous

polarization. There are many mechanisms which ferroelectricity can originate from such as, polar groups such as NO_2^-, hydrogen bonds as in KH_2PO_4, polarisable lone pairs of Pb^{2+} and Bi^{3+} or small ions in large octahedra. Many perovskites are ferroelectrics and among them, the alkali metal niobates and tantalates [48-53]. In perovskites a common mechanism for ferroelectricity is d^0-ions such as Ti^{4+} and Nb^{5+} inside a too large coordination polyhedron as in e.g. $BaTiO_3$ and $LiNbO_3$. In these oxides the mechanism for ferroelectricity is the displacement of the oxygen octahedra relative to the transition metal between two stable positions along the polar axis [54]. In the $LiNbO_3$ structure the polar axis is along the c-axis [54] and the stable positions of the Nb^{5+} ions are close to the faces of the octahedra which are perpendicular to the c-axis. Another common mechanism for ferroelectricity in perovskites is the lone-pair displacement of the 6s electrons for Bi^{3+} and Pb^{2+}, which is responsible for the ferroelectricity of bismuth- and lead-based ferroelectrics as $BiFeO_3$ and $Pb(Zr,Ti)O_3$.

The applications of ferroelectrics are many, but FeRAM is important [55, 56]. In FeRAM the permanent storage of charge is used to store a “1” or a “0” as either the positive or negative remanent polarization. The large advantage of FeRAM is the low power consumption and the non-volatile nature. The ferroelectric will remain polar when the field is switched off and therefore do not need power to store information causing less heat evolution and more robust storage.

3 Atomic layer deposition

One of the ways materials can be designed on the nanoscale is as thin films. The applications of thin films are diverse, and range from corrosion and wear protection of tools to reflecting aluminium layers in mirrors, food packaging or electronic devices. These different applications require different materials and different tolerances. For instance in food packaging a diffusion proof layer that lasts for some weeks may be enough, while semiconductor devices needs several layers of different materials where thickness, composition, crystal structure, orientation, morphology and other properties are controlled carefully, and the device should have a lifetime of many years.

Materials deposited as thin films span all classes and properties of materials, from metals to insulators, from single elements to complex oxides and from amorphous materials to highly epitaxial layers and super-lattices. Also the methods for making thin films are very varied. The methods are often divided into physical methods which are based on evaporation of a material for instance by a direct heat, laser pulses or sputtering with highly energetic ions, and chemical methods which rely on a chemical reaction either in the liquid phase as spin coating or from the gas phase as chemical vapour deposition (CVD) or atomic layer deposition (ALD).

In this work, samples have been synthesized using ALD. Although ALD is also well known in the literature, a description is given in order to compare the growth of alkali metal compound to better known processes.

The ALD technique was patented in 1974 and was originally developed for industrial production of thin film electroluminescent displays [57]. The electroluminescent displays are still in production today, almost 40 years later. ALD is also used extensively by the microelectronics industry for deposition of high-κ dielectrics [58], metallization [59] and MEMS devices [60, 61] . New technologies are also being developed which can utilize the advantages of ALD on industrial scale in more mundane applications such as strengthening of glass [62], gas and moisture barrier coatings [63-65] and corrosion protection [66, 67].

A typical ALD-process runs at relatively low temperature. Most processes can be run somewhere between 100-400^{o}C, but many processes work all the way down to room temperature, while others work at much higher temperature. The low deposition temperature possible in ALD allows the use of substrates such as plastics and polymers [63, 64, 68, 69] in addition to ceramic-, metal-, glass- and semiconductor substrates which are normally used. The types of materials which can be deposited by ALD span almost all material classes, from single elements [70-74] to oxides [75-78], nitrides [79-84], phosphates [85-87], silicides [88], carbides [89], sulphides [90-92], selenides [93], tellurides [93, 94] and fluorides [95-100]. The materials can be deposited as amorphous, polycrystalline or epitaxial or with different orientations depending on deposition temperature [101-103], substrate [102, 104-108] and other processing conditions [109-111].

The underlying principle behind ALD is a series of consecutive self-limited solid-gas reactions, separated in time or space if the substrate is moving [65, 112]. As an example an imaginary material AX is to be deposited by a thermal process. In this process, precursor A-R is a molecule containing a metal and precursor H-X is a molecule that contains the anion, normally water or ozone for deposition of oxides, ammonia for deposition of nitrides or TMPO for the deposition of phosphates, and so on. The role of precursor A is therefore to provide the cation of the deposited material and the role of precursor X is to supply the anion by ligand exchange, and in some cases reduce or oxidize the metal. The precursor X can also be ozone or a plasma which combusts the ligand and releases combustion products from the ligand. In a typical ALD-cycle a vaporized precursor, A-R, is pulsed into the reactor chamber. The precursor reacts with the surface which is to be covered until the surface is saturated with precursor A, and the reaction reaches a steady state regime. After the pulse, the reaction chamber is purged of un-reacted precursor before the surface is exposed to the next precursor, H-X, which forms AX on the surface and releases H-R. After this step the chamber is purged of H-X and H-R. This sequence, A/purge/X/purge, is called an ALD-cycle. At ALD-conditions the number of adsorbed precursor molecules on the surface is constant, and therefore the growth per cycle is also constant. Therefore, the thickness can be predicted exactly from the number of cycles, and the cycle is then repeated until the desired film thickness is obtained.

True self-limiting reactions can only take place when there are no side reactions as such as etching, precursor desorption or thermal decomposition of the precursors [113]. The

temperature interval where the self-limiting reactions occur is called the "ALD-window" and is often assumed to have a growth rate which is constant with temperature. The important feature of the ALD-window is that the reactions are self-limiting, not that the growth rate is constant. In fact, most "text-book" ALD-processes do not have a constant growth rate at different temperatures, but are still ALD-processes [114-116].

ALD can also be used to deposit films that consist of more than two elements. In order to deposit a compound $A_pB_qX_{p+q}$ sub-cycles of AX and BX are mixed so that the total cycle becomes (n(A+X)+m(B+X)). The problem of relating n and m to p and q, i.e. the relation between the pulsed stoichiometry and the stoichiometry which is deposited, can be solved by measuring the elemental content in the film for different pulsed ratios. The required values for n and m can to the first approximation be estimated from the ratio of the growth rates of AX and BX. The models by Lie [117] and by Elliott [118] can then find the desired stoichiometry. Another option for deposition of ternary compounds is to use a bimetallic precursor; that is a precursor which contains more than one element.

The self-limiting surface reactions give rise to some intrinsic advantages and disadvantages of ALD. The main disadvantage of ALD is often considered to be the growth rate. As the film thickness is dependent on the number of cycles, the film thickness obtained per hour is dependent on the length of a cycle. The cycle length is typically between one second and 30 seconds and the growth rate per cycle is normally in the range of 0.1-2Å per cycle. When compared to other deposition techniques, ALD is therefore is often considered quite slow. On the other hand, the advantage is that the area which can be coated by a single pulse is in principle only limited by the size of the deposition chamber and therefore the batch size can be very large. Batch sizes in the order of tens of wafers can be run routinely or in some cases up to 250 wafers [119] or 1000 wafers [120] depending on wafer size and the specific process is advertised. The large batch size can therefore make the total production volume per day very large. Due to the purge step there are no gas-phase reactions, and the deposited films are in principle particle free, and particles which are already on the surface is covered by the film, thus depositing, in principle, pinhole free films. Another advantage is that the films are extremely uniform, thickness variations of <1Å on a 12" wafer is obtainable [58, 121], as the growth per cycle is the same everywhere in the reactor.

ALD is also one of the few thin film techniques which can be used to deposit thin films inside high aspect ratio surfaces. As there are no reactions between the precursors the aspect ratios can routinely be as high as 100, or even as high as 1000 [122], depending on the reactor design and process. ALD can also be used to deposit thin films onto powders with the same accuracy [123, 124].

These properties make ALD ideal for depositing insulating layers and for applications in batteries. In ferroelectrics and battery electrolytes there cannot be any pinholes or the device will short circuit or self-discharge. In batteries applications, a thin film battery will benefit from being deposited on a high aspect ratio surface such as the "*3D-integrated all-solid-state battery*" mentioned above [29]. For such a battery to be realized, a complete set of materials for a lithium ion battery must be developed for cathodes, anodes and electrolytes into a process which can be deposited on high aspect ratio substrates.

3.1 Applications of ALD in battery research

Atomic layer deposition has been suggested for use in battery research as a way to study electro active materials [125-128], as a means to deposit entire battery structures [29] or in order to enhance the performance of bulk electrodes [123, 124, 129].

Lithiated cathode materials such as $LiMn_2O_4$ [125] and $LiCoO_2$ [130] have been deposited by ALD and their electrochemical performance have been evaluated. Also many of the transition metal oxides with potential as cathodes in lithium ion batteries have been deposited; however lithium intercalation studies have only been performed in a few cases. The vanadium oxides have been subject to extensive studies, both Le *et. al.* [131] and later by Badot *et al.* [132, 133], Chen *et. al.* [134-136] and Pomerantseva *et al.* [137]. In all these studies $VO(O^iPr)_3$ has been used as vanadium precursor, however depending on the process conditions either crystalline [134] and amorphous films can be deposited. There is no clear consensus on the optimum parameters for a vanadium oxide based cathode as the experimental details for the electrochemical studies vary. Generally, if the cathodes are cycled in the high voltage region, *i.e.* the lower voltage is above 2.5 V, the crystalline cathodes have longer lifetime than their amorphous counterparts. If the cathodes are cycled to about 1.5 V the cycling stability of the cathodes suffers, but the amorphous cathodes are more stable, but requires very slow cycling

speeds. There is also a general trend that thinner films gives better capacity retention and faster cycling speeds.

$Li_4Ti_5O_{12}$ is the only lithium containing anode material which has been deposited using ALD [126, 138], however there are still no reports on the electrochemical performance of the thin films. Other oxide thin films have been studied with respect their performance as anodes in lithium ion batteries. SnO_2 anodes deposited using plasma-ALD have been reported show capacities in the order of 365 mAh/g when cycled up to 0.8V, in this range, no degradation of the anodes are observed after 500 cycles [139]. TiO_2 anodes are shown to have good lifetime and good rate capabilities [140].

As described above, one of the intrinsic properties of ALD is the ability to cover all exposed surfaces inside the reaction chamber. This ability is advantageous when coating powders, as the film covers the surface of the powder with a uniform layer. The performance of bulk electrodes can be enhanced by surface coatings through different mechanisms. Better electronic conductivity, modified surface chemistry, HF-removal, physical protection, lower dissolution of the cathode and solvent decomposition [129, 141, 142] have been listed as possible mechanisms, depending on coating material. The most utilized material for performance enhancement of cathodes is Al_2O_3. Al_2O_3 is an insulator and a lower total electronic conductivity of the cathode is observed when the cathode is covered with Al_2O_3 [142], on the other hand the stability of the material increases. When the coating is sufficiently thin the advantages of high stability outweigh the drop in conductivity. Typically 2-4 ALD-cycles of TMA + H_2O, which corresponds to 0.25-0.5 nm appears to be the ideal thickness of coatings on $LiCoO_2$, 10 cycles (1.2nm) was found to be the optimal thickness on $LiMn_2O_4$ cathodes [143] and 6 cycles on $Li(Li_{0.2}Mn_{0.54}Ni_{0.13}Co_{0.13})O_2$ [144]. Other materials have also been utilized, such as TiN on $Li_4Ti_5O_{12}$ anodes which showed better capacity at high C-rates [145], ZnO on $LiCoO_2$ was found to yield poorer performance than Al_2O_3 [142] and recently TiO_2, Al_2O_3 and ZrO_2 films with different thicknesses on $LiCoO_2$ were compared and supports the notion of 2-4 cycles of Al_2O_3 as the ideal coating [146].

3.2 Deposition of lithium and other alkali metal compounds with ALD

The field of lithium in ALD-processes have recently been reviewed [147], but will be also be briefly summarized and commented here. Since the first report of a proof of concept for

lithium based processes, many different lithium containing materials have been reported such as lithium oxides [104, 126-128, 148, 149], -fluoride [98, 99], -nitride [80], -carbonate [80], -silicate [86] and –phosphate [86]. The applications are mostly centred on materials for lithium ion batteries, but in this work ferroelectrics are also shown to be an application of lithium based ALD [104].

The different materials also require different types of precursors, and a large range of precursors have therefore been explored. The precursors in the literature which are reported to work for deposition of lithium based materials are shown in Table 1. There are also a large range of other potential lithium compounds which are investigated as precursors, but which do not work for deposition due to low vapour pressure or low temperature thermal decomposition [86, 148].

The properties of the reported lithium precursors, such as deposited materials, reactivity and vapour pressure can be linked to the composition and structure of the precursors. One obvious difference between these precursors is their composition. For instance when LiHMDS is used with ozone it will deposit $Li_xSiO_{2+x/2}$ [150], while Li(thd) will deposit Li_2CO_3 with ozone [148]. Similarly, the purity of the films depends on the composition of the precursor, as the Li(thd) and LiO^tBu may leave significant carbonate contamination and LiHMDS yields high amounts of silicate when used with ozone and hydrogen impurities when used with water [104].

Table 1 Summary of reported processes for lithium containing materials

Precursor name	Evaporation temperatures	Deposition temperatures	Materials deposited	References
Li(thd)	175-200°C	180-300°C	Li_2CO_3	[98, 125,
			Li-La-O	148]
			LiF	
			$LiMn_2O_4$	
LiO^{t}Bu	90-160°C	225-275°C	Li_3PO_4	[86, 125,
			$LiAlO_2$	126, 128,
			$Li_4Ti_5O_{12}$	130, 149]
			$LiMn_2O_4$	
			$LiCoO_2$	
			$LiTaO_3$	
LiHMDS	60-90°C	89-380°C	$LiNbO_3$	[80, 86,
			Li_3N	104, 150]
			Li_2CO_3	
			Li_3PO_4	
			$Li_xSiO_{2+x/2}$	

The structures of these compounds are quite diverse, and there can also be significant differences between gas, solid, liquid or solvated state. LiHMDS is a dimer in the gas phase and liquid phase and a trimer in the solid state [151, 152]. LiO^{t}Bu is reported to exist as a hexamer in the solid state [153] and in gas phase [154, 155]. Li(thd) on the other hand is reported to be tetrameric in the gas phase[156]. The degree oligomerization of these compounds is a compromise between increasing the coordination number of the alkali metal and the steric hindrance of the ligand. The degree of oligomerization will affect the evaporation temperature of a compound, as the evaporation temperature is to the first approximation proportional to the molecular mass, and will be modified by the intermolecular forces [157]. By utilizing the size of the gas phase cluster it is possible to find a clear correlation between the molecular mass and the reported evaporation temperature as shown in Figure 3. This correlation does not take any thermodynamical parameters into account, but helps to rationalize the relatively high precursor temperature needed for evaporation of alkali metal compounds. For instance, the sublimation temperature of Li(thd) is in the same range as

$La(thd)_3$ [158] , which is surprising when only comparing the formula weights. When the tetrameric structure of the lithium compound is taken into account, the molecular weights for these two compounds are also comparable.

The composition and structure of the ligand determines the pK_a, which governs the materials which can be deposited. The high pK_a in the range of 26-36 makes the free O^tBu- and HMDS-ligands superbases [159]. The high affinity for protons makes LiHMDS able to strip protons from ammonia [80] and both the HMDS and O^tBu can take methyl groups from TMPO [86] and protons from water [80, 104]. The thd ligand on the other hand has a pK_a in the range of 7-9 [160], and therefore requires ozone as precursor. Apparently, the ligand largely determines the possible products. The lithium containing materials deposited with ALD are already quite diverse, and there is reason to believe that a similar diversity can be obtained with sodium and potassium.

The precursors for sodium and potassium share many of the properties of the lithium analogues, however there are some differences. For the HMDS compounds the Li- and NaHMDS are reported to be covalent compounds while KHMDS is considered as ionic [151]. NaHMDS is polymeric in the solid state [161], and monomeric in the gas phase [162] which makes the compound under coordinated, and unstable in the gas phase. KHMDS is a dimer in the solid state [163] and to the best of knowledge there is no reported gas phase structure. From TGA-data there is reason to believe that KHMDS decompose rather than evaporate [164]. The large structural variation in this series is dependent on both the metal centre and the state of the compound. This difference is probably the explanation for the difference in usability between LiHMDS and the sodium and potassium analogues. The *tert*-butoxides and silanolates of all the alkali metals form four to nine-membered cages with four coordinated metal atoms at half the vertices and alkoxy or silanolate groups at the other vertices. These structures are found in the solid state structures and the known gas phase structures [165-168]. Where lithium *tert*-butoxide forms cages with six lithium atoms per cage, sodium forms cages with either six [164] or six and nine sodium atoms and potassium forms cages with four potassium atoms per cage [165-168]. These molecules with four-coordinated alkali metals are also thermally stable as the usable temperature interval for this group of precursors is quite large. The sodium precursors seem to fit the pattern in Figure 3, and KO^tBu is an outlier in the proposed relationship. From the evaporation temperature of KO^tBu, it is tempting to suggest that it exists as a hexamer as well. However, as all other experimental evidence is against the

hexamer model, the explanation for the discrepancy is probably stronger interactions between the cages, arising from the more ionic character of the potassium-oxygen bond.

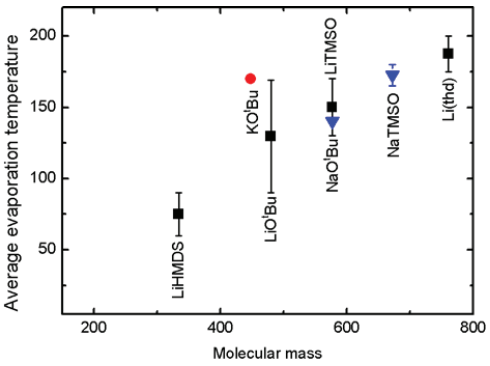

Figure 3 Correlation between reported evaporation temperature values of lithium precursors and total molar mass of the complexes, the data is assembled from Table 1 and [154-156, 164-168]. Black markers correspond to lithium, blue to sodium and red to potassium compounds.

It has previously been speculated if true ALD growth of lithium compounds is impossible due to the single positive charge of lithium and this causes lithium to exist as complexes with only one ligand [148], if true this would also extend to other alkali metals. This is however not the case as shown for example for LiO^tBu which exist as a hexamer [153, 154, 169] in the gas phase and LiHMDS exists as a dimer in the gas phase [152], as described previously. Therefore this cannot be the origin of the differences between lithium processes and other processes.

How are alkali metal processes different from other processes?

The application of lithium processes can in practice be somewhat different compared to other ALD-processes. Lithium is a quite unusual metal when compared to most of the other *p*-, *d*- and *f*-block metals, especially in terms of mass and charge. The low mass and size contributes to a relatively high mobility in most matrixes [170, 171]. Also lithium is restricted with respect to bonding as only the *s*-orbital is available. The alkali metals also have a higher affinity for water and CO_2 than most other elements.

The high affinity for CO_2 and water is a challenge, as mentioned above. The affinity for carbonate is mainly problematic as a purity issue, and the alkali earth metals readily forms carbonate impurities or main phases when deposited using ozone [106, 172]. Carbonate contamination can be removed by annealing the sample at high temperature [172], by using

precursors which reacts with water [173, 174], or in some cases a stable phase can suppress the formation of carbonates [107, 117]. The tendency to form carbonates is also present among the lanthanide oxides [175].

The high affinity for water on the other hand opens the discussion if true ALD growth is possible with lithium and the other alkali metal compounds. If water is used a precursor in lithium processes the lithium oxide will absorb water to form LiOH, possibly with a significant amount of crystal water in the material [176, 177]. This ability to "store" water between the pulses has become known as the "reservoir effect" [178, 179] as the deposited film acts as a reservoir of water. The excess water will then react with the subsequent metal pulse and hence lead to an increased growth rate from the subsequent pulse. As shown by Aaltonen *et. al.,* the growth rate of $LiAlO_2$ depends on the number LiO^tBu cycles preceding the TMA-pulse [128]. The increased growth rate probably arises from the amount of water present in the film. There may also be a slow release of the water during the purge and the subsequent metal pulse, which may disrupt the ALD-growth and cause inhomogeneous thickness profiles and particle formation. Comstock *et al.* has shown by QCM-analysis of LiOH-growth that after a nucleation period, a large mass gain during the water pulse occurs and a slow decrease in mass during the purge as well as conversion of LiOH-films to Li_2O-films after 10-20 min in vacuum at 300 ^oC. Cavanagh *et al.* have shown in a similar experiment that the deposited film continues to lose mass for two hours after the last water pulse at 225 ^oC [177]. A similar case is described by Vehkamäki for the growth of barium compounds. Vehkamäki showed that thin films of crystalline barium hydroxide or barium oxide capped with Al_2O_3 can be deposited. Depending on the deposition temperature and waiting time before capping different phases of $Ba(OH)_2$ or BaO can be obtained. $Ba(OH)_2$ may contain up to nine equivalents of water, however only one crystal water left above 110 ^oC [180], thus it is uncertain if the material on the surface is $Ba(OH)_2$ or $Ba(OH)_2{\cdot}H_2O$. The deposited film releases water from hydroxide ions and crystal water to form the oxide after one hour in vacuum at 340^{o}C [174], however there were no tests of exactly how fast this release was.

There is an indication of a limit to how many hygroscopic metal ions which can be incorporated into an ALD-surface. In the case of $BaTiO_3$ growth from $Ba(^tBu_3C_5H_2)_2$, $Ti(OMe)_4$ and water, the maximum ratio between barium and titanium cycles which yielded

stable films was 1:1 which also corresponded to a stoichiometric ratio of barium and titanium in the film [174]. For $LiAlO_2$ growth from LiO^tBu, TMA and water the 1:1 ratio between LiOH and Al_2O_3 cycles is found also deposit a 1:1 ratio which is the maximum content which can be incorporated while retaining linear growth [176]. Aaltonen has verified that a 1:1 ratio of LiO^tBu, TMA and water results in linear growth at 225 ^oC. $Li_4Ti_5O_{12}$ can be deposited from LiO^tBu, $Ti(O^iPr)_4$ and water with any ratio up to 2:1 Li:Ti with no significant change in growth rate and the deposited films can contain up to nine times more lithium than titanium. In this work the limit to how much lithium which could be safely incorporated into niobium oxide was found to be every third cycle of LiHMDS and $Nb(OEt)_5$ i.e. a 1:2 ratio [104], and for sodium aluminate every second cycle of NaO^tBu and TMA while for potassium aluminate every third cycle of KO^tBu per cycle of TMA, corresponding to a 1:3 ratio of deposited potassium gave stable growth [164].

In a textbook ALD-process the surface hydroxyls thought of as only bound to the actual top layer of atoms, however in processes containing hygroscopic metal oxides the surface may mean the top few atomic layers. The surface required for ALD-growth contains some reactive surface sites, normally hydroxyls, for growth of Al_2O_3 from TMA and water, the amount of surface hydroxyls will be limited by the number of Al^{3+}-ions on the surface, which is where the hydroxyls are bound. If the deposited material can form hydroxides or take up crystal water, such as Li_2O, the total number of reactive sites can be larger than what would normally be fit in a single layer on the surface, as for instance in the case of Al_2O_3-growth. The larger amount of accessible water will then yield a higher growth rate of the next cycle compared to the previous cycle. If the amount of water is too large the reservoir of water can potentially increase with the volume of the film, *i.e.* exponentially, and the process is no longer surface controlled. As discussed above, there seems to be a limit to the amount of cations which readily forms hygroscopic compounds which can be deposited. The limit of appears to be about half of the total metal ions in the film, with the exception of potassium aluminate and lithium titanate. A suggestion to the origin of this limit is that the balance between the cations which do and do not form hygroscopic compounds. The (sub)-stoichiometric amounts of cations which do form hygroscopic materials are stable, and if they are in excess the growth gets uncontrolled. Therefore materials with stoichiometric or sub-stoichiometric amounts of hygroscopic metal oxides will display ALD-growth, as the precursors are not decomposing and the surface actually controls the growth. However the remaining challenges are that the

excess hydroxide must be released during the purge. The implications are that the process optimization or reactor design and the coating of high aspect ratio substrates may be more challenging, due to the purge step.

Most of the applications for lithium processes are deposition of materials for lithium ion batteries. The deposited materials will therefore, normally, lithium ions which to some degree are mobile. Considering that the depositions happen at elevated temperatures, the lithium will be even more mobile in the film during deposition than after. The mobility of lithium inside the films after deposition is evidenced by lithium enrichment at surfaces [104, 128]. The mobility during deposition is evidenced by intercalation of lithium from the gas phase as in the case of deposition of $LiMn_2O_4$ and the intercalation of lithium into V_2O_5 [125] or exchange of magnesium with lithium in the transformation of MgF_2 to LiF by Li(thd) [99]. The two cases described above both signify the mobility of lithium and the latter also suggests that Mg^{2+} ions are also mobile. The reactions in the two examples are probably quite different. In the transformation of MgF_2 to LiF there is a ligand exchange between the lithium ions in the gas phase and the magnesium ions in the film with a subsequent evaporation of $Mg(thd)_2$. Surprisingly, crystalline LiF is the product. In the case of the manganate and vanadate, there is an intercalation of lithium into the structure, and probably a reduction of the transition metal ions by the ligand. These processes may be better described as a transformation or reaction than a film built up by atomic layers. Still, the processes retain the properties of an ALD process. The uniformity and coverage of 3D-structures and so on, are guaranteed as the film body, the MgF_2, MnO_2 or V_2O_5, is still deposited using ALD. These processes are not surface limited in the same way as conventional ALD-processes; they are rather limited by the film body. In this sense they are still self-limiting although the space inside the structure, instead of by the number of sites on the surface.

The high mobility of lithium also partially constrains which characterization techniques which can be used to determine lithium content. Several methods have been used such as XPS [21, 128], ICP-analysis [128] and ion beam analysis as TOF-ERDA [86, 104, 125, 150] or nuclear reaction analysis [130] have been utilized to determine the lithium content, however there is normally a discrepancy between these techniques. Enrichment of lithium at surfaces will cause XPS-measurements to yield a higher value of the lithium content, and sputtering during XPS will cause an unphysical depth profile due to mobile lithium ions. The safest and most robust method appears at the moment to be ion beam analysis.

The implications of the highly mobile lithium ions and the possible reduction of transition metal ions by the ligands set some limitations to how thin film lithium ion batteries can be designed. First the control of the total amount of lithium in the battery is important. The total lithium content of the deposited cathode and anode must correspond to a fully charged battery, in order to exploit the full capacity. This requires a good control of the lithium stoichiometry and implies that some of the transition metal ions in the cathode or anode will be deposited in a reduced oxidation state. For realization of the 3D-battery using ALD, it appears that the best substrate is a structured silicon substrate. $Li_4Ti_5O_{12}$ is recently reported deposited by ALD [126, 138] and is a good anode for thin film batteries due to the low volume expansion during cycling [5]. A promising candidate as a solid electrolyte, amorphous lithium tantalate, is recently reported; however it is not yet tested in a battery [149]. For the cathode $LiMn_2O_4$ or V_2O_5, which is lithiated after deposition, is suggested. This scheme will deposit a fully discharged battery and will also enable annealing of the anode before deposition of the electrolyte and cathode. As an added benefit, when using a 3D-substrate, the water used for the anode and the electrolyte is used when the pores are at their largest - causing the least problems with purging the excess water out of the pores.

4 Methods for characterization

This chapter will describe some of the characterization methods used in this work. The emphasis is put on x-ray scattering and ellipsometry and electrochemical characterization. These methods described here have contributed to the bulk of the results and have been used most extensively in this work. This section describes briefly the principles behind the methods used, while the details of each experiment can be found in the experimental sections of the papers.

4.1 X-ray based methods

The x-ray based methods used in this work are either scattering techniques, such as diffraction (XRD) or reflectometry (XRR) or spectroscopic techniques such as fluorescence (XRF) and photoelectron spectroscopy (XPS). The spectroscopic methods are not used to the same extent as scattering and therefore only scattering methods will be described here.

X-ray scattering is one of the ways that x-rays can interact with matter. In a scattering process the interaction is elastic and thus the wavelength for the incident and the scattered beam is the same. A scattering experiment is normally performed by shining x-rays with a known wavelength and direction onto a material and measuring the intensity of the scattered radiation at different values of the scattering vector **Q**, which is defined in Eq. 1. The length of **Q** corresponds to the scattering angle, 2θ, and direction corresponds to the angles between the incident beam and the sample, ω.

$$\mathbf{Q} = |\mathbf{k_0} - \mathbf{k'}| \qquad \text{Eq. 1}$$

A general feature of scattering experiments is that the intensity obtained is the square of the Fourier transform of the structure that scatters the radiation. As the Fourier transform includes a complex number, squaring expression implies that the phase information is lost and the full interpretation of the data can only be performed by modelling and data fitting.

X-ray reflectometry measurements normally refer to measurements of the specular reflectivity at low incident angles, normally below 5-8 degrees. An interesting feature of x-ray reflectometry is that the refractive index in the x-ray range, which is given by Eq. 2, is slightly less than unity.

$$\tilde{n} = 1 - \delta - i\beta \qquad \textbf{Eq. 2}$$

In Eq. 2 ñ is the complex refractive index, δ is a number in the range of 10^{-5} and β is the absorption coefficient. A refractive index less than unity give rise to the phenomenon of total external reflection. The reflected x-rays from the interfaces in the sample interfere, causing what is known as *Kiessing fringes* which can be used to determine the thickness. In measurements of x-ray reflectivity the contrast comes from the derivative of the electron density as shown if Eq. 3. The electron density can then be interpreted as the thickness, roughness and the density of the deposited layer, or layers in the case of a multilayer.

$$I(q_z) = \frac{1}{q_z^4} \left| \int \frac{d\rho(z)}{dz} e^{(iq_z z)} dz \right|^2 \qquad \textbf{Eq. 3}$$

The software packages used to fit the data (GENX or Reflectivity) use a description of the sample called Parrat's exact recursive formalism [181] which separates the reflected intensity into intensity from infinitely thin strata in the sample and then sums over all strata to obtain the total intensity.

X-ray diffraction is also a scattering technique, but the scattering here comes from atoms positioned on crystalline lattice sites instead of from interfaces. The signal is again a Fourier transform, but in this case of the product of the Fourier transforms of the lattice and the atomic motif of the sample. The vectors spanning the reciprocal space is described by Eq. 4, where **G** is the reciprocal space vector, *h, k* and *l* are the Miller-indices of a plane and $\mathbf{a_1}^*$, $\mathbf{a_2}^*$and $\mathbf{a_3}^*$ are the unit vectors of the reciprocal space.

$$\mathbf{G} = h \cdot \mathbf{a}_1^* + k \cdot \mathbf{a}_2^* + l \cdot \mathbf{a}_3^* \qquad \textbf{Eq. 4}$$

There is a relation between planes in real space and points in the reciprocal space which gives rise to the Laue condition for diffraction is given in Eq. 6. The Laue condition states that diffraction occurs if the scattering vector is equal to a reciprocal lattice vector, **G**.

$$\mathbf{Q} = \mathbf{G} \qquad \textbf{Eq. 5}$$

The Laue diffraction condition could be reduced to the familiar Braggs law, which is shown in Eq. 6.

$$2d \sin \theta = n \lambda \qquad \textbf{Eq. 6}$$

The direction of the incident beam, i.e. the ω-angle, will matter if the sample shows some preferred orientation. A symmetric reflection, that is a reflection belonging to a lattice plane parallel to the sample surface, will only be brought into diffraction condition when the angle between the incident beam and the sample, ω, is half of the scattering angle 2θ. An asymmetric reflection is one that belongs to some other plane which is not parallel to the surface.

The diffracted intensity from a single crystal will in the ideal case be distributed as points in the reciprocal space. However, effects such as strain, disorder, particle sizes and mosaicity will change the shape of the intensity. In most cases a film deposited at low temperature is not epitaxial or even crystalline. The most common case is polycrystalline films which can be treated as a powder which will either be randomly oriented or show some type of preferred orientation and in these cases the intensity is distributed on concentric spheres or rings in the reciprocal space, respectively. Different types of samples will therefore call for different measurement geometries and the demand for resolution depends on the information needed. For example, will a randomly oriented film benefit from grazing incidence geometry; however for a textured sample it is most beneficial to use a symmetric scan. Measurements of epitaxial films will be a combination of symmetrical scans and scans of separate reflections. More thorough measurements of the intensity around the reflections, referred to as reciprocal space maps (RSM), will give information of the particle size and mosaicity and the position of the reflection will give information on the exact lattice parameter and the strain in the film.

4.2 Ellipsometry and optical methods

Ellipsometry has been used extensively in this work for determining thicknesses and refractive indices of deposited materials. In some cases UV-VIS spectroscopy has been used to establish boundary conditions for fits of the ellipsometry data of vanadium oxide and infrared (IR) spectroscopy has been used to determine the impurities of hydroxyl and carbonate in sodium and potassium oxides.

Optical methods utilize the fact that materials, depending on their electronic configuration, will have different interactions with radiation of different wavelengths. An easy example is shown in Figure 4, with pictures are taken of a rainbow with visible light and infrared light. From the pictures it is obvious that infrared light behaves similarly to visible light, however the refractive index is slightly lower for IR-light so rainbows are shifted slightly. The concept of colours does not make real sense outside the visible range; however, in spectroscopy the "colour" is described as the energy or wavelength of the photons. The absorption of light comes from an interaction between the photons of light and the electrons in the sample. For radiation around the visible range, these interactions can be the band gap of the material or d-metal absorption, for infrared light the interaction can be absorptions from functional groups such as carbonate or hydroxyl groups. All these interactions are described by the dielectric function of the material:

$$\varepsilon = \varepsilon_1 + i\varepsilon_2 \qquad \textbf{Eq. 7}$$

By determining the absorption of light, and determining the optical properties and dielectric function, detailed knowledge of the material, such as the presence of impurities, the band gap and dopants can be inferred.

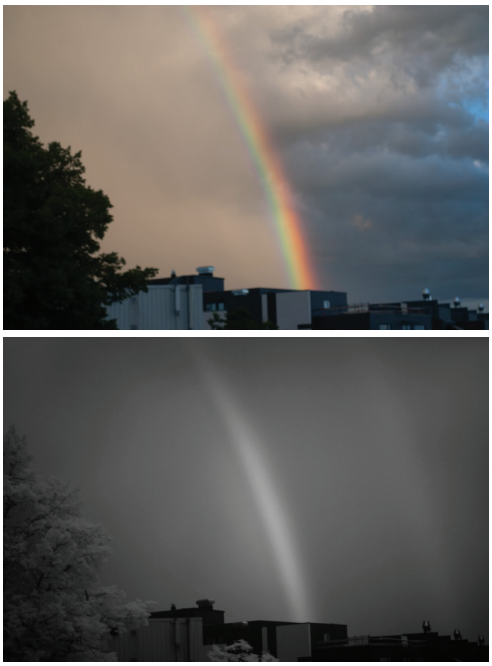

Figure 4 Hyperspectral photographs of a rainbow over Oslo with (from top) visible light and 900-1100nm showing that the rainbow extends into the IR-range. The images are not processed except for a normalized exposure and transformed into black and white.

The way materials changes polarization of light can be used to determine the optical properties and the thickness of the deposited films. Most light sources such as incandescent light bulbs, the sun and LED's emit unpolarised light which means that all polarization states are present and a polarization filter is needed to polarize the light. Some sources, such as lasers can directly emit polarized light. Another example is again shown by the rainbow photographed with different polarization directions in Figure 6. A light beam can be described by an oscillating electric field, which involves a propagation direction, amplitude frequency and phase. The polarization of the beam is given by the direction of the electrical field vector and the phase. There are two special cases of polarization, linear and circular. If the x- and y-components of the electric field are in phase the light has a linear polarization, and if they are 180^{o} shifted the light has circular polarization. Between these special cases the light is elliptically polarized.

As the polarization is a vector, it can be decomposed into two components, the $E_{p,}$ the component parallel to the plane of incidence and E_{s}, perpendicular to the plane of incidence.

When a polarized light beam is reflected by an interface there is a change in the reflected intensity and phase between the two components, R_s and R_p. In an ellipsometry experiment the beam is polarized at an angle to the surface as shown in Figure 5. When a polarized light beam interacts with a material there is a change in intensity of the two components, R_s and R_p. The ratio between the two intensities are known as tan Ψ and given as:

$$\tan \Psi = \frac{\left|R^p\right|}{\left|R^s\right|} \qquad \textbf{Eq. 8}$$

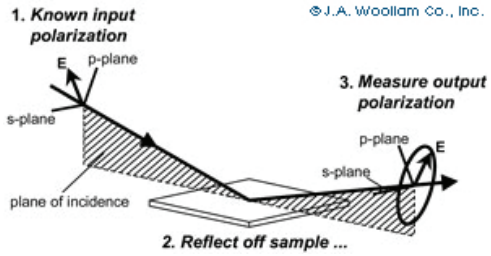

Figure 5 Principle of operation for an ellipsometer showing the geometry and how the sample changes the polarization from linearly to elliptiacally polarized light the picture is taken from[182]

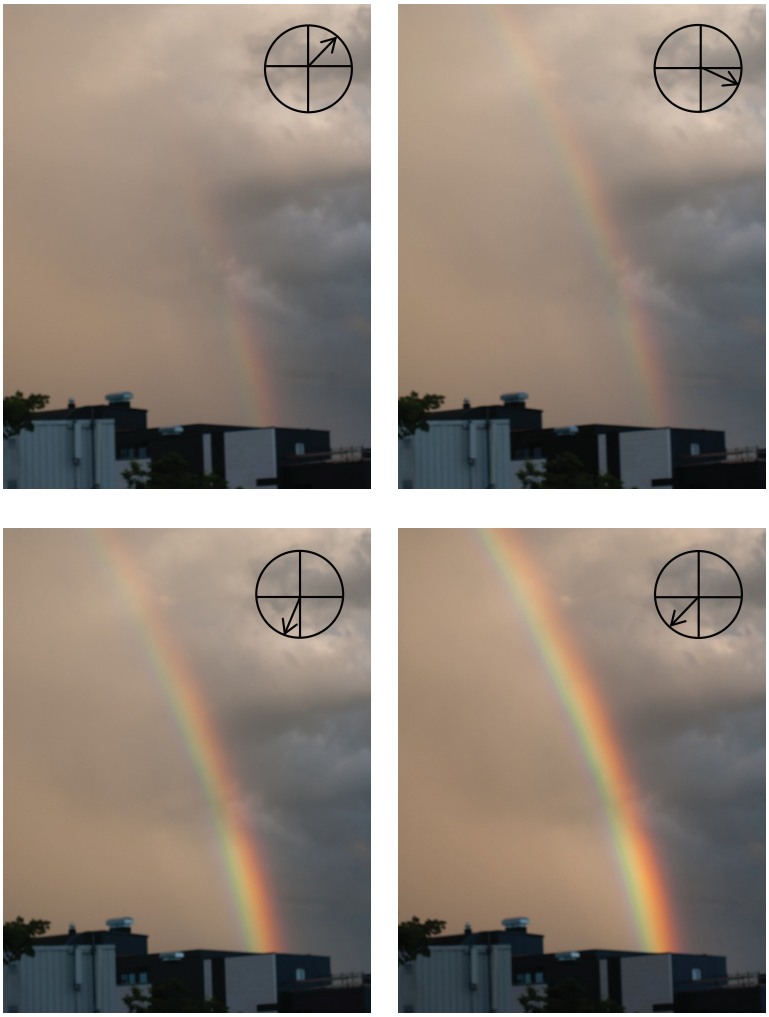

Figure 6 Photographs of a rainbow over Oslo taken with a circular polarization filter with different rotation directions of the polarizer illustrating the difference in intensity for the different components of the light. The images are cropped.

The absorption of light will affect the phase difference of between the R_s and R_p components which is described as Δ. The whole interaction of the polarized light can then be described by the fundamental equation of ellipsometry:

$$\tan \Psi e^{i\Delta} = \frac{R^p}{R^s} \qquad \textbf{Eq. 9}$$

In a spectroscopic ellipsometry tan Ψ and Δ are measured as a function of wavelength and possibly also incident angle which enables simultaneous determination of the both thickness and optical properties. The experimental parameters such as incident angle and wavelength, and the derived parameters such as thickness and optical properties of the sample are included in the R^p and R^s.

Simultaneous determination of the thickness and optical parameters of the sample is not completely straight forward as there is no unique solution to Eq. 9 and R^p and R^s are in general complex numbers. The thicknesses and optical constants must therefore be determined by constructing a model of the film and fit free parameters to the data. Normally the best strategy for obtaining the film thickness is to determine an energy range where k = 0, i.e. the film is transparent, as this reduces the number of complex factors in the calculations. The data can then be fitted to the Cauchy function in Eq. 10 where n(λ) is the refractive index as a function of the wavelength of the incident beam, while n_0, n_1 and n_2 are the fit parameters. If n(λ) is known the thickness normally can be determined easily.

$$n(\lambda) = n_0 + \frac{n_1}{\lambda^2} + \frac{n_2}{\lambda^4} \qquad \textbf{Eq. 10}$$

Determining the absorption or the dielectric function of the material can then be performed by first obtaining the thickness and then iteratively including data into a B-spline function [183] which is an arbitrary smooth function which fits the data. This B-spline function can then be used as a starting point for modelling the dielectric function through the use of oscillators which describes the polarisability of the material with physically meaningful parameters. The different types of absorption which must be included in the model is for instance the band gap, d-metal absorptions and the free carrier absorption, depending on the energy range investigated.

4.3 Electrochemical characterization of cathodes

Characterization of the electrochemical properties of V_2O_5 has been performed using cyclic voltammetry and chronopotentiometry. This chapter will describe some terminology and the techniques used in this part of the work.

The electrochemical characterization is performed in a coin cell. The coin cells are assembled as shown in Figure 7, and top and bottom are pressed together in order to seal the cell. The material studied is used as a cathode and cycled against a lithium metal foil. In this thesis a liquid electrolyte is used in all experiments. The cells are assembled inside a glove box as the lithium foil and electrolyte are air sensitive.

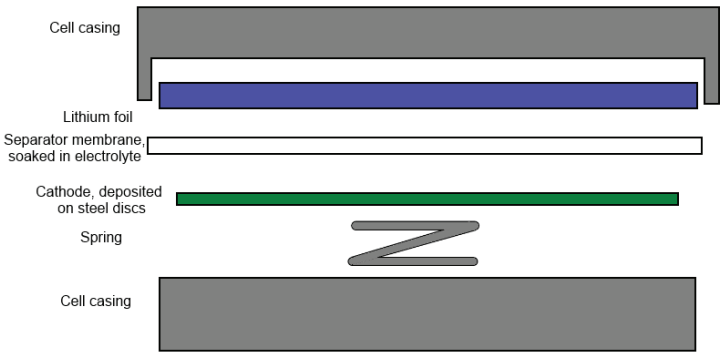

Figure 7 Drawing of the coin cells used in characterization of the electrochemical properties

In order to compare the performance of batteries it is customary to compare the capacity of the battery. Normally this is done in the amount of charge the battery can store per unit weight, as is done here by using mAh/g, or by unit volume or area which can be useful in the case of a thin film battery. An interesting parameter is the speed of which a battery can be charged or discharged. In order to compare the discharge current of different materials the C-rate is often used. The C-rate is defined so that 1C is one discharge per hour. From the definition it follows that 0.1C equals 0.1 discharges per hour or 10 hours per discharge and 60C equals 60 discharges per hour or one discharge per minute, and so on. The voltage of the battery is also an interesting parameter. The voltage is dependent on the redox-pairs in the cathode and anode. The voltage will however change during discharge of the battery. From the charge and the voltage of a battery the power and energy densities can be calculated.

Voltammetry is the measurement of a current during a voltage sweep and cyclic voltammetry (CV) refers to series of voltammetry measurements where the voltage is swept back and forth. When performing voltammetry on an electrochemical cell the current is monitored while the voltage is changed in order to charge or discharge the cell. An increased current will be observed when the voltage corresponds to the voltage associated with the redox pairs in the electrode which is under investigation. There might be several peaks in the voltammogram for

a single redox pair which is caused by the different free energies associated with intercalation of lithium into different sites in the structure. Changing structural environments and difference in diffusivity due to phase transitions will change the appearance of the voltammogram for successive charge discharge cycles, however ideally the voltammograms should not change.

Chronopotentiometry or galvanostatic cycling is the application of a current pulse while measuring the voltage required for keeping that current. The current is chosen according to the desired C-rate and kept until the desired threshold voltage is reached.

In order to characterize an electrode material a combination of CV and galvanostatic measurements will be performed. Typically a CV will be performed first with a slow scan speed before the cell is subjected to galvanostatic cycling at different C-rates.

5 Summary and discussion of the results

This section will summarize and discuss the results of the experimental work in this thesis. First the part of the work concerned with deposition of vanadium oxide is summarized and discussed (paper I and II). Then the part of the work concerned with ALD of lithium compounds is summarized discussed (paper III-VI), before finally the work with sodium and potassium oxides are treated (paper VII-VIII). The chapter is concluded with a discussion of the evidence of redox reactions on the surface and a comparison between lithium, sodium and potassium processes.

5.1 Work with vanadium oxide based processes

The motivation for the part of the thesis concerned with vanadium oxide was to make a thin film cathode based on vanadium oxide. When assembling a battery and using an un-lithiated metal oxide as cathode, the metal should normally be in the highest possible oxidation state. Preparing the oxide in a high oxidation state will give the possibility of intercalating the highest number of lithium ions, which gives the largest capacity. This first part of the results describes the development of a high power cathode of V_2O_5 using ALD. By utilizing a new vanadium precursor $VO(thd)_2$, a process for depositing thin films of crystalline V_2O_5 with a highly textured surface is developed. The morphology of the surface is strongly dependent on the deposition temperature as shown in Figure 9. Depending on the number of ALD-cycles used the preferred orientation of the films change. The process conditions were optimized so that the films consisted of a single layer of nano-platelets which showed unprecedented lifetime and cycling speeds when cycled in a battery vs. lithium.

Paper I describes the growth and optical characterisation of V_2O_5 from $VO(thd)_2$ and ozone. The growth dynamics of this system is quite complex, and a thorough investigation was conducted and presented in paper I. It is hypothesized in paper I that a catalytic combustion of the precursor occurs at some crystal facets. The growth rate is too large to be explained by the size of the precursor, regardless of the number of ligands used in the calculations, however QCM-experiments verifies that the process is self-limiting. The anisotropic growth rate of different crystallite surfaces can also be explained by the catalytic reaction. Depending on the temperature, the growth rate is in most cases higher for samples deposited with 2000 cycles than with 500 cycles, as shown in Figure 8. The growth rate of the films is not only dependent

on the deposition temperature, but also on the number of deposition cycles. It is speculated in paper II that the crystallites oriented with the fastest growing direction normal to the surface will dominate for thicker films. This result could also be obtained through modelling of the growth.

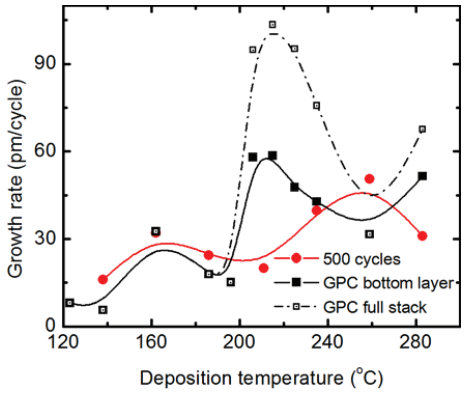

Figure 8 Growth per cycle of V_2O_5 from $VO(thd)_2$ and ozone vs. Temperature for 500 ALD-cycles (red dots) and for 2000 cycles black dots. Open and closed symbols signify the full thickness of the films and the dense bottom layer, respectively [103]

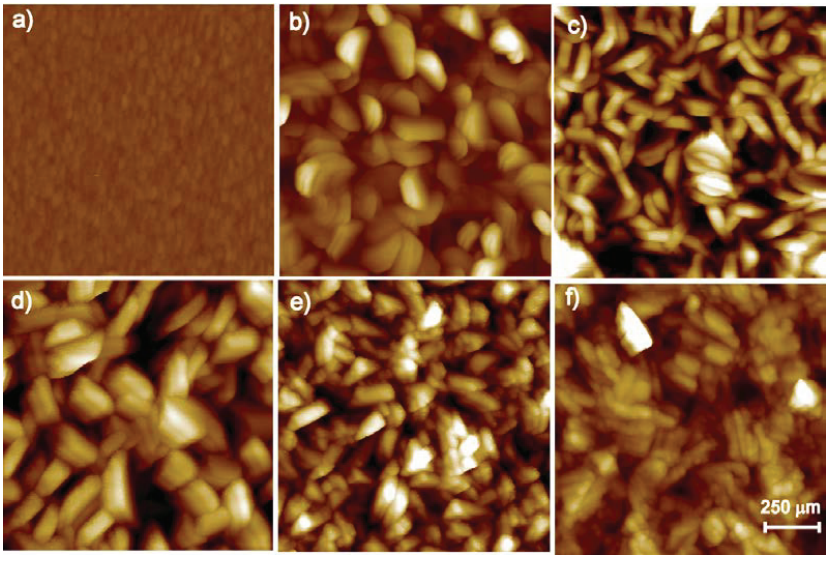

Figure 9 AFM images of thin films deposited using 2000 cycles at different temperatures a) 162 °C, b) 186 °C, c) 206 °C, d) 215 °C, e) 236 °C and f) 283 °C . The height scale is ±40 nm except for e) and f) where the height scale is ±75 nm.

Determining the thickness of the films was far from trivial as the surface roughness was very high, as shown in Figure 9. A method for using spectroscopic ellipsometry was found to be useable after the realisation that the films were a combination of a dense part and a relatively thick surface layer as indicated in the sketch in Figure 10. The surface layer has the same properties as the dense part, but also consists of some fraction of air. The theory is already well known in the literature and is named the Bruggemann effective media approximation (BEMA) [184]. In paper II the method for measuring thickness was verified by exactly reproducing the thickness derived from ellipsometry with measurements of the deposited mass from XRF.

For BEMA to be effective, the dielectric function is also needed. In paper I, the dielectric function of the V_2O_5 films was parameterized using a model based on two Lorentzian oscillators. The oscillators are assumed to represent transitions over the optical band gaps in the material. The model corresponds well with the band structure of V_2O_5 and with the band gaps extracted from UV-VIS spectroscopy. The band gap varies slightly with deposition temperature, but a direct band gap is found at 2.6±0.1eV and an indirect band gap at 2.25±0.1eV.

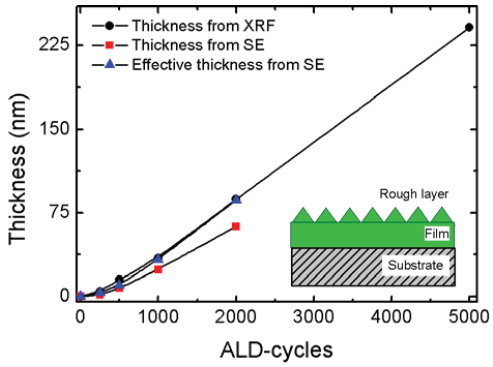

Figure 10 Effective thickness of films deposited on silicon at 215 °C [185]. The thickness derived from XRF and ellipsometry are compared. The inset is a sketch of the model used to determine the thickness.

It was found that ALD-growth of amorphous films could be obtained at 162°C and crystalline samples could be deposited from 186°C and up to the limit of self-limited growth at 267°C. The crystalline samples showed strong texture and very rough surfaces, with surface roughness up to 50 nm for a 200 nm thick film. Films were normally textured with preferred

orientation along the *b*-axis up to 200°C and along the *b*- and *c*-axes at temperatures up to 225°C, and for samples deposited at the highest temperatures where the films became more or less randomly oriented. In paper II it was found that the texture also depends on the number of cycles. At 215 °C, the films are oriented along the *c*-axis until 500 cycles before *b*-axis-reflections appear at 1000-2000 cycles and random orientation is found above 5000 cycles. The catalytic reaction mentioned above explains this change. This reaction will cause different growth rates for different crystal facets. The crystallites oriented with the fastest growing direction normal to the surface, i.e. the *b*-axis will therefore dominate the surface for high number of cycles as they overgrow the other crystallites oriented in other directions.

After the growth dynamics of the V_2O_5-films were understood, the films were developed into a high power density cathode for lithium ion batteries, which is described in paper II. The aim was to make the roughest possible surface as this would promote the area in contact with the electrolyte which again would promote the transport of lithium into the material. Figure 11 shows schematically how a rough surface of the same thickness has more contact points to the electrolyte; the thicker film has fewer grains in simultaneous contact with both the electrolyte and the current collector. A series of samples with different thickness were then deposited at 215°C, which was found in paper I to yield the largest surface roughness. The fact that the samples would, at least for thin samples consist of more or less free nano particles was thought to have a positive impact on the electrochemical performance.

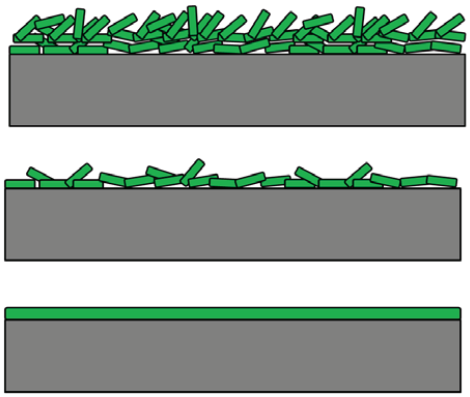

Figure 11 Schematic drawing which compares, (from bottom to top) a thin amorphous film, thin nano crystalline film and thicker nano crystalline film.

The electrochemical characterizations revealed that all samples showed relatively good electrochemical performance when cycled between 3.75 and 2.7 V vs. Li/Li^+. All samples were stable for at least 75 cycles when cycled at 1 C and the samples were exposed to varying discharge speeds between 1 C and 10 C. The samples deposited using 500 cycles showed only a small decrease in capacity at a discharge rate of 10 C. These samples were then investigated more thoroughly and discharged at different rates between 1C and 960C as shown in Figure 12. In order to test the long term stability of the samples they were exposed to 4000 charge/discharge cycles at 120 C, which corresponds to 30 s charge and discharge. The battery endured more than 1500 cycles before dropping below 80 % of the original capacity, as shown in Figure 12. The battery could still take charge after 4000 cycles, although the battery was permanently damaged and had decreased capacity which did not recover when cycled at slow speeds. It is likely that the sample has such a high performance because it contains freestanding nano particles of V_2O_5 which results in short diffusion length for lithium and good electric and ionic contact with the current collector and electrolyte, respectively. The current collector also works as a heat sink, which is an important factor as the current per gram of material is in the range of 140A/g when discharged at 960 C, which would vaporize a bulk cathode.

When comparing the results obtained in paper II with the literature, is appears as if these results are comparable to the best results reported for V_2O_5-cathodes with respect to cycling speeds and cycling stability. The combination of high rate performance and long term stability reported is unprecedented. This is a promising result for use of V_2O_5-cathodes in thin film batteries as the high stability will give a long lifetime of the device. The high power density can be used to build a device with a small battery which gives the same power as a much thicker battery.

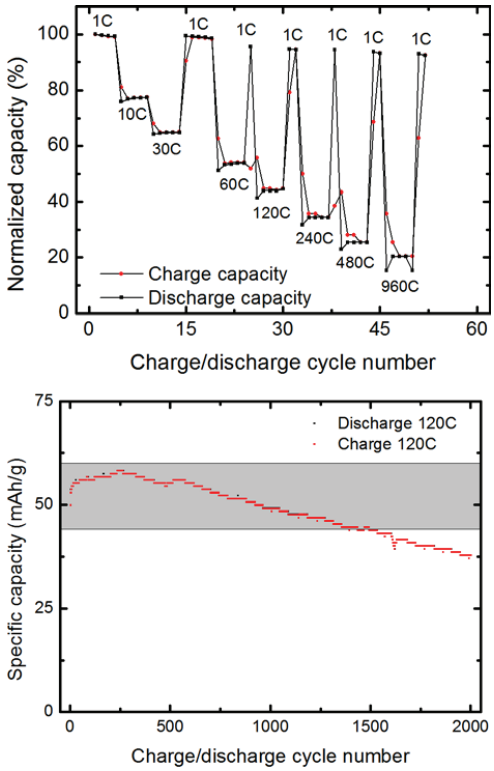

Figure 12 Top: High rate test; bottom: cycling stability test of V_2O_5 cathode deposited using 500 cycles at 215 °C

5.2 Work with lithium ALD

This section describes the part of the work concerned with direct deposition of films that contain lithium. The relevant papers here are papers III-V.

Paper III describes the use of LiHMDS as precursor for deposition of lithium nitride and lithium carbonate. The motivation for this part of the work was threefold; first the deposition of Li_3N is potentially interesting for future depositions of LiPON. Secondly, a part of the work was also originally planned to be on nitrogen doped oxide cathodes and therefore a process for Li_3N was tentatively important. Finally it was interesting to develop LiHMDS as a precursor for lithium oxides; Li_2CO_3 was used as a model system for oxides. The use of

LiHMDS was chosen as the silylamide group is extremely alkaline and is capable of stripping protons from ammonia.

The first part of paper III describes the growth of Li_2CO_3 from LiHMDS, H_2O and CO_2 at temperatures from 89°C to 332°C. The deposited films are crystalline from 186°C to 332°C, and amorphous when deposited outside this temperature range. It was also found that the growth of Li_2CO_3 required relatively long pulses of both LiHMDS in order to achieve saturation and CO_2 in order to completely convert the deposited LiOH to Li_2CO_3. The long LiHMDS pulses are probably required as the Li_2CO_3 surface is poor in -OH groups and hence quite unreactive. The growth per cycle of Li_2CO_3 is lower at higher temperatures inside the ALD-window, which is rationalized as the packing density of the LiHMDS precursor on the surface and not –OH-group density. At low temperatures, such as 89°C, the surface species probably packs in a quite dense fashion as the temperature does not provide the necessary energy for free rotation of the surface species and the growth rate is about 0.41 Å/cycle. As illustrated in Figure 13, packing without free rotation will cause the precursor to occupy an area shaped as an ellipse. At higher temperatures such as 289 °C the molecules are free to rotate, *i.e.* occupy a circular area, and thus lowering the packing density resulting in a growth rate of 0.23 Å/cycle. The deposition of Li_3N was found to achieve saturation much faster than in the case of Li_2CO_3. Pulses of only one second for both LiHMDS and ammonia were sufficient to achieve saturation when depositing Li_3N. The reaction is probably faster because of the higher reactivity of the amine-terminated surface than the carbonate surface.

Characterization of the deposited Li_3N films were challenging as both lithium and nitrogen interacts quite poorly with x-rays and the material is very air sensitive. When exposed to air, the films turned milky white within the span of a few seconds. To increase the lifetime of the samples, they were capped with a layer of MoN_x and it was also found that the reproducibility of the samples were better when a nucleation layer of MoN_x was deposited first. The capping layer increased the lifetime up to a few days before the samples deteriorated, which gave sufficient time for characterization of the samples. The MoN_x layers also had the advantage that they enhanced the contrast in XRR-measurements.

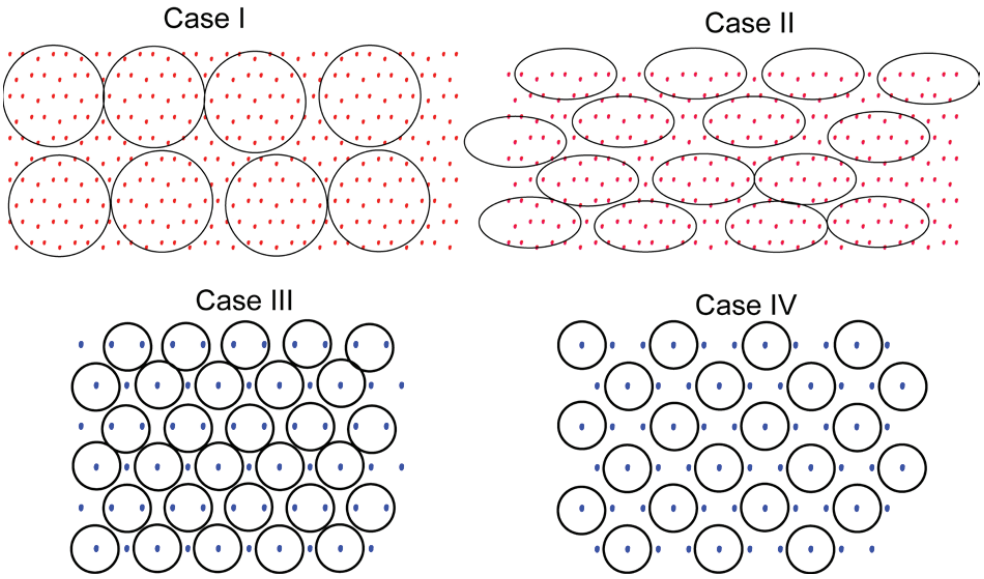

Figure 13 Different models for packing of LiHMDS-molecules on Li_2CO_3 (Case I-II) at high and low temperature, respectively, and on Li_3N (Case III-IV) [178].

Both Raman-spectroscopy and x-ray diffraction proved the existence of both the α- and β-Li_3N phases. The diffractograms also revealed the existence of impurities of hydroxides and carbonates. The growth per cycle of Li_3N is relatively high, around 0.95 Å/cycle at 186 ^{o}C. When applying the same arguments as presented for the growth of Li_2CO_3 the growth rate could again be reproduced theoretically, see case III in Figure 13. The surface reaction is thought to proceed through proton transfer between amine-groups on the surface and the LiHMDS-dimer and the subsequent release of a HMDS-group. This reaction is quite fast and selective as the deposited films are almost free of silicon from the ligand.

At this point in the work there was an emerging pattern both in the work performed by other members of the research group and in the literature that deposition of thin films containing lithium, which contained p-block-elements such as $LiAlO_2$, Li_3PO_4 and $Li_xSiO_{2+x/2}$ worked quite well, while deposition of compounds containing transition metals as $LiFePO_4$ and $LiMn_2O_4$ did not work exactly as expected. Some preliminary attempts of deposition of compounds in the Li-Mo-O-N system also failed. In order to explain this pattern, a hypothesis was then formulated: the problems connected with deposition of lithium-transition metal compounds come from the ability of the transition metal to change oxidation state and hence

intercalate lithium into the film during growth. A necessary criterion for this hypothesis is that the carbon in the precursor ligand reduces the transition metal. The reduction will seem like a decomposition of the lithium precursor, which is not self-limited in the classical sense, but is limited by the volume of the film body. Further, the high mobility of lithium allows the lithium to distribute evenly inside the sample. From this hypothesis it follows that deposition of $LiNbO_3$ should behave "as the p-block compounds as pentavalent niobium does not reduce to the tetravalent state with carbon. Therefore it should be possible to deposit $LiNbO_3$ with a normal approach to ALD.

In paper IV the success with the LiHMDS precursor was explored further through the deposition of $LiNbO_3$. A process for deposition of $LiNbO_3$ was then developed using LiHMDS, $Nb(OEt)_5$ and water as precursors. Figure 14 shows that it was possible to deposit samples with controllable Li-Nb contents from pure Nb_2O_5 up to a lithium content of about 70 % as measured with TOF-ERDA. The pristine films were characterized by ellipsometry and the refractive index proved to be a good figure of merit for the lithium content, as shown in Figure 14.

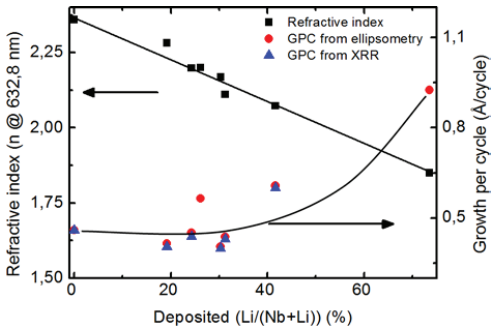

Figure 14 Refractive index and growth per cycle for Li-Nb-O-films deposited using LiHMDS, $Nb(OEt)_5$ and water for varying ratios of niobium and lithium.

The stoichiometric phase $LiNbO_3$ was also successfully deposited when combining two pulses of $Nb(OEt)_5$ with one pulse of LiHMDS. This ratio was then used to deposit amorphous films, which crystallized into phase pure $LiNbO_3$ after annealing at 650°C. Films were then deposited onto several different single crystal substrates such as Al_2O_3, $SrTiO_3$, $LaAlO_3$ and silicon and epitaxial films were obtained on Al_2O_3-(001) and (012) as well as $LaAlO_3$ (012)

after annealing. The annealed films were also proven to be ferroelectric when deposited on silicon. Hysteresis loops were collected on samples deposited on silicon, the remanent polarization was found to be 0.4μC/cm^2 and the coercive field was found to be 220kV/cm. These values are consistent with the congruent composition.

It was also discovered that two consecutive depositions, with the same cycle ratio between lithium and niobium, never gave the same result, especially for films rich in lithium, unless the reactor was passivated with Nb_2O_5 between the depositions. This suggests that the films contain some mobile lithium ions that can give rise to the reservoir effect which resulted in enhanced growth rate and poor uniformity. Considering that amorphous lithium niobate is a good lithium ion conductor [24] it is not unexpected that this could occur. However, the lithium content could be controlled for a transition metal oxide of lithium, so the prediction from hypothesis that lithium niobate is possible to deposit is tested.

In-situ XRD annealing experiments of $LiNbO_3$ showed that the lithium is mobile at high temperature. In-situ experiments were performed using x-ray diffraction where the intensity of the 006-reflection was monitored as a function of temperature and used as a measure of crystallinity, as shown in Figure 15. As expected there are different onsets of the crystallization with different heating rates. However, it was unexpected that the intensity dropped to zero when heated to ~700 ^oC. The loss of crystallinity is ascribed to evaporation of lithium from the film, and supports the notion that lithium is very mobile in these samples.

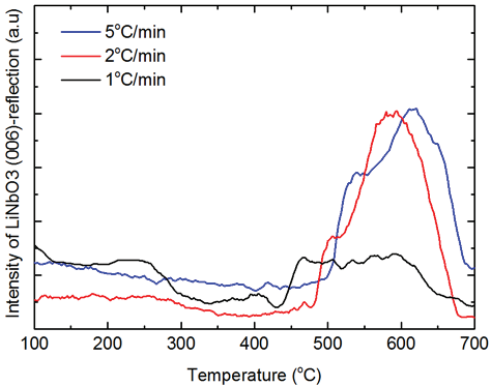

Figure 15 Intensity of the 006-reflection of $LiNbO_3$ deposited on c-Al_2O_3 when heating up to 700 ^oC with varying heating rates.

In paper V the hypothesis of intercalation of lithium into transition metal oxides where the oxidation state could be changed was tested. $LiMn_2O_4$ was deposited from $Mn(thd)_3$, Li(thd) or LiO^tBu and ozone and/or water, respectively. It was found that the lithium mangante spinel could be deposited by using any pulsed ratio of manganese to lithium between 1:99 and 1:19. This ratio is unusually low for deposition of a complex oxide, and it should be a relation between the deposited content and the pulsed content. This finding strengthened the belief in the hypothesis as it suggests that the ALD-growth during the lithium cycles in this system is not limited by the surface species, as is the case for normal ALD-processes, but by the bulk of the film. In order to really test the hypothesis films metal oxides that were thought to be able to intercalate lithium and get reduced, such as for instance V_2O_5, Co_3O_4 and MnO_2, as well as some films that were thought not get reduced as ZnO and Al_2O_3 was exposed to Li(thd) and LiO^tBu vapours inside the ALD-reactor. This treatment caused intercalation of lithium into V_2O_5 and MnO_2 thin films and which formed $Li_xV_2O_5$ and $LiMn_2O_4$, respectively, when exposed to Li(thd) and ozone or LiO^tBu and water.

In order to test if a redox reaction happens and to control the stoichiometry, deposition of lithium manganese compounds from a divalent manganese precursor ($Mn(EtCp)_2$) was attempted. The idea was that the divalent manganese ions would not get reduced by the lithium precursor, and that the process should be similar to the lithium niobate. The film could then be annealed in oxygen after deposition in order to crystallize the desired phase. Regardless of the lithium precursor the film thickness decreased with increasing amount of lithium pulses and no lithium was found in the film after deposition. Both LiHMDS and LiO^tBu was attempted, but both precursors showed either etching or growth inhibition of the manganese precursor, resulting in little or no film growth, as shown in Figure 16. Also depositions using sodium in place of lithium was then performed using NaO^tBu with a similar result. No sodium was found in the films and all the films were profiled with a strong gradient along the flow direction.

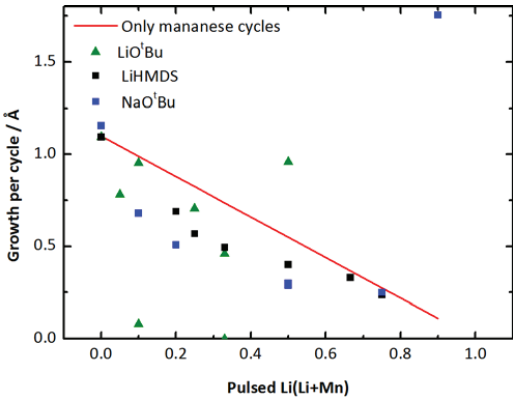

Figure 16 Growth rate versus pulsed stoichiometry of sodium or lithium in the $Mn(EtCp)_2$ + H_2O-process showing decreased growth rate when the alkali metal precursors are pulsed.

5.3 Work with other alkali metal processes

The work done with lithium processes provided the inspiration for developing processes for sodium and potassium oxides. In order to fully understand the chemistry of lithium processes, deposition of sodium and potassium compounds are important. Especially to understand to which degree the mobility of the lithium ions in the film affects the growth and how the reservoir effect works and being able to check hypotheses with sodium or potassium processes may is important. As the ionic radii of sodium and potassium are significantly larger than for lithium and they will therefore be less mobile in the deposited films. Thus it provides an opportunity to study ALD-chemistry of monovalent elements with less diffusion than what is the case for lithium. It is also worth mentioning that the other alkali metals scatter x-rays stronger and it is possible to get good and fast compositional analyses using XPS or XRF without having to rely on the heavy infrastructure of ion-beam measurements. Thin films of sodium and potassium compounds could also have potential as piezo- and ferroelectric materials and thin film sodium ion batteries.

In paper VII the first depositions of sodium and potassium oxides are reported. Six different precursor candidates were evaluated, and the main findings are that sodium and potassium oxides can be deposited with ALD, using the respective *tert*-butoxide compounds. The candidate precursors that were evaluated were the sodium and potassium *tert*-butoxides, trimethyl silanolates (TMSO) and hexamethyldisilazane. Of these six candidates, only the

tert-butoxides and the sodium silanolate were found to evaporate cleanly, the other compounds yielded a black residue and left a high residual mass – suggesting thermal decomposition before evaporation, as shown in Figure 17.

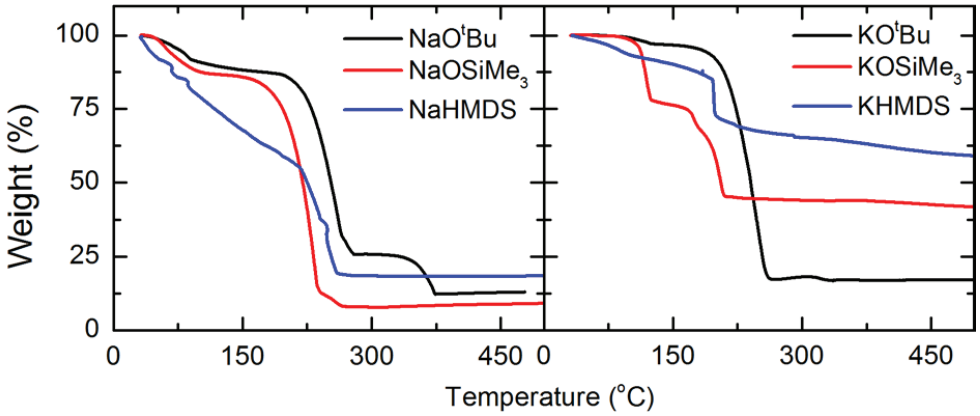

Figure 17 TGA of the candidate precursors for sodium and potassium oxides performed nitrogen atmosphere at a heating rate of 2°C/min [164].

Sodium silanolate was tested as a single source precursor for deposition of sodium silicate in a reaction with ozone. The films always displayed gradients in thickness and the refractive index along the direction of the flow, suggesting that the composition is different along the flow direction. It was clearly not a saturation issue as the gradient in thickness and refractive index was independent of the precursor dose. The most probable cause is therefore a side reaction which poisons the surface; however this was not explored in detail. The silanolate was also tested with water as reactant and combined with the TMA/H_2O process, but this did not remedy the gradients, nor did using another tool.

From experience and literature on lithium processes, it was considered that the pure sodium or potassium oxides and hydroxides would not be obtainable due to the reservoir effect and reactions with ambient CO_2. To circumvent this problem and in order to be able to evaluate the precursors, the sodium and potassium *tert*-butoxide processes were combined with the TMA-water and the TMA-ozone process. The sodium and potassium *tert*-butoxides on proved to be robust precursors which, when mixed with the TMA-water or TMA-ozone process showed saturation and gave uniform films, before scaling up to 8”-wafer scale. An ALD-

window was found from 225°C to 375°C for sodium and 225-300°C for potassium. It was also found that the stoichiometry could be controlled, as expected from an ALD-process, as shown in Figure 18. The high sodium or potassium regions were not explored. The samples were all amorphous as deposited.

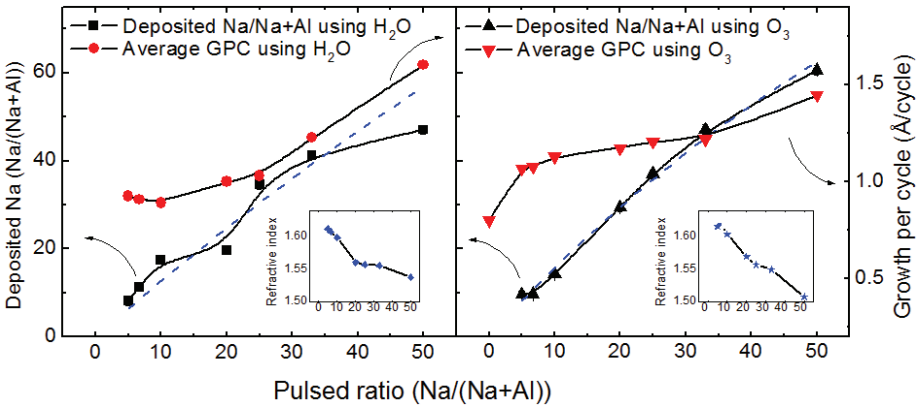

Figure 18 Growth rate, composition and refractive index for samples deposited using NaO^{t}Bu and TMA and water (left) or ozone (right).

After a robust set of precursors for sodium and potassium was developed, the work was extended into deposition of more interesting materials. The deposition of lithium niobate was already known and a natural path was then to compare the alkali metal processes through deposition of niobates and tantalates. In paper VIII the deposition of perovskites of sodium niobate and tantalate are explored. The paper shows that the chemistry developed in paper VII is transferrable to other complex oxides.

It was found that amorphous thin films of both sodium and potassium niobate could be obtained on silicon, and epitaxial $NaNbO_3$ could be obtained on $SrTiO_3$ substrates when deposited at 250 °C. When attempting to crystallize films deposited on silicon, the films also turned amorphous when heated further after crystallization. As shown in Figure 19, a similar effect was found for $NaNbO_3$ as was found for $LiNbO_3$. When heated above ~475 °C the films crystallized very fast. If the heating was continued to over 500 °C, the intensities of the reflections decreased before vanishing completely. This is also ascribed to loss of alkali metal; however it unexpected as thin film deposition of these compounds is routinely performed at much higher temperatures [186].

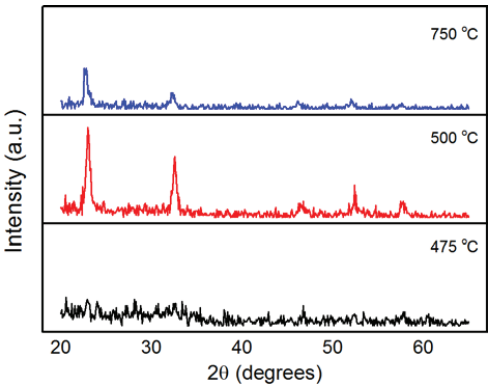

Figure 19 Crystallinity of $NaNbO_3$ deposited on silicon when annealed at different temperatures, obtained by in-situ high temperature GIXRD.

5.4 Redox reactions on the surface

Possible surface redox reactions are found in this work, both the process for V_2O_5 and the $LiMn_2O_4$ process indicates this behaviour. In the V_2O_5 process the growth rate is too high to be explained by the relatively large size of the precursor, even though the process is demonstrably self-limiting. In the $LiMn_2O_4$ process the redox reaction is thought to be the cause of the uniform lithium incorporation. The generally accepted "textbook" reaction mechanism occurring in ALD consists of precursor absorption on the surface and subsequent ligand exchange reaction with water to form the oxide and a gaseous by-product [187], these processes are in general well understood and described[188]. For an ozone process the simple ligand exchange does not occur, but to the first approximation is that the ligand gets oxidized by a pulse of ozone and forming the oxide and combustion products from the ligand. However, for ozone based processes there is significant dispute in the literature on the mechanism even for simple process as the TMA and ozone process, where the experimental and theoretical models do not agree [189, 190], and the mechanisms for ozone processes can be quite complex [179]. Theoretical studies of ozone based processes are also scarce, see [191] and references therein, and experimental studies of the reaction mechanisms and chemistry of ozone processes are also rare, see [192] and the references therein. It is established in the literature that ozone combusts the ligand and for some processes leaves a surface covered with hydroxyls and/or chemisorbed active oxygen [192]. It should also be noted that many of the transition metal oxides can be used as oxidation catalysts for

hydrocarbons. If the metal can easily change oxidation states, such as vanadium or manganese, the redox mechanism may play an important role in the growth chemistry of even binary oxides.

5.5 Comparison of the alkali metal ALD-processes

It is interesting to contrast and compare the ALD-chemistry of lithium to that of sodium and potassium. It appears that some of the basic features of the lithium processes are similar, such as the tendency to form carbonates and hydroxides. By extension the reservoir effect, should also occur in these kinds of processes. In the case of an ozone based process, the surface redox could not be excluded, but the intercalation of sodium and potassium from the gas phase would likely be suppressed as the larger size of sodium and potassium reduces the diffusivity of these ions compared to lithium. The processes for sodium and potassium appears to be more stable and easier to control than lithium processes, however this is hard to quantify.

The precursors evaluated for sodium and potassium are analogues of known lithium precursors. However the HMDS-complexes of sodium and potassium do not behave as the lithium analogues – which probably arise from their structures being different. The silanolates are not well known, but it is surprising that they are very different from the *tert*-butanol-complexes. In the case of the *tert*-butanol-complexes, the precursor chemistry is similar as the molecular structures of the precursors similar and the chemistry of the elements are also similar, but the ionic radius is quite different.

6 Conclusion and future perspectives

In this thesis the development of a high power cathode of V_2O_5, the exploration of LiHMDS in order to develop processes for Li_3N, Li_2CO_3 and $LiNbO_3$, deposition of $LiMn_2O_4$ as well as deposition of sodium and potassium compounds such as the Na-Al-O and K-Al-O and $NaNbO_3$ have been discussed. These subjects are chemically somewhat different from each other; however, they are all steps on the way to improve lithium ion battery technology by ALD.

Two different ways to incorporate lithium ions into thin films have been explored; either by directly depositing the lithiated material or incorporating lithium electrochemically into V_2O_5. These methods are in general the only two ways to incorporate lithium into the cathode and they differ quite a lot when designing the process. Direct deposition of materials containing alkali metals is shown for lithium, sodium and potassium. In the cases of alkali metal niobates, tantalates and aluminates, this route has been quite successful. It is hypothesized that direct deposition of materials which contains alkali metals is possible when there is no reaction between the ligand of the lithium precursor and the deposited material.

The process for V_2O_5 has been used to develop a thin film cathode with very high power density and long lifetime. The combination long lifetime, fast cycling speed and high power density is among the best of what is reported in the literature. The results suggest that V_2O_5 could be used as a cathode in future thin film batteries. The results also imply that bulk cathodes of V_2O_5 could be optimized further to yield longer lifetime and higher power densities. If this material is integrated into all solid state thin film batteries, there is good promise that the cathodes will have even longer lifetime due to the solid electrolyte. The "*3D-integrated all-solid-state battery"* is probably also even more important than previously thought. While thinner cathode is probably normally beneficial thicker cathode with respect to power density and lifetime, a thicker cathode is superior with respect to energy density per area. While the performance of the reported cathodes already bridges the gap between batteries and supercapacitors with respect to power and energy density, the benefit of these findings can be even greater if the energy density per area can be increased by another order of magnitude by utilizing the "*3D-integrated all-solid-state battery."* It is also probable that the effect of a thin cathode is not exclusive to V_2O_5, and therefore ALD should be used to

explore the thickness effect of other potential cathode materials with the aim of determining the optimal cathode for the "*3D-integrated all-solid-state battery."*

The deposition of lithium containing materials is still not a mature field. The deposition of lithium manganate has also been studied in this work and has given new insight into the chemistry of lithium processes. In the $LiMn_2O_4$ process the lithium precursor reduces the manganese ions and the spinel phase which is formed is so stable that it does not oxidize once formed A new mechanism for incorporation of lithium has been suggested, and hopefully this opens up for use in other systems. Lithium manganate is also the first lithiated cathode material deposited by ALD, and therefore a key to the "*3D-integrated all-solid-state battery."*

In this study, LiHMDS has been used to deposit lithium nitride, carbonate and niobate which have further increased the available chemistries for lithium in ALD-processes. This opens up for deposition of a number of complex oxides, or complex nitrides for anodes. Amorphous lithium niobate should also be investigated with respect to ionic conductivity, as the tantalate was recently shown to have ionic conductivity. Especially since the present results suggests that the lithium ions are quite mobile in the lithium niobate films.

The lithium niobate was shown to be ferroelectric when deposited on silicon, and epitaxial when deposited on different single crystal substrates. Different epitaxial relationships could be obtained depending on the orientation of the substrate. Sodium and potassium oxides have been deposited for the first time. Many different precursor candidates have been investigated, and processes for aluminates and niobates have been developed. The deposition of amorphous $NaNbO_3$ both silicon and epitaxial on single crystal substrates are also shown. The deposition of alkali metal based ferroelectrics is promising for the use of ALD to deposit lead-free ferroelectrics.

The deposition of sodium and potassium compounds is still in its early days and should be explored further. The work with sodium and potassium oxides would hopefully be developed further to realize proof of concept sodium batteries and sodium and potassium based ferroelectrics. *In situ* studies using quartz crystal microbalance and spectroscopy should be performed, in order to work out the mechanisms and comparison to the growth of lithium compounds would yield useful insights. A number of interesting transition metal oxides could

also be investigated such as Na_xCoO_2 and other materials with potential as electrodes for sodium ion thin film batteries.

Contributions to specific papers

I. Optical properties of V_2O_5

The author conceived the idea to the project. Planned and performed the synthesis, x-ray and AFM characterization and organized the interpretation of the results. The author participated in the electrochemical characterization and the interpretation of the results. Organized the writing process and finalized the manuscript for publication.

II. Ultrafast V_2O_5 cathodes for thin film micro batteries by ALD

The author conceived the idea to the project. Planned and performed the synthesis, x-ray and AFM characterization and organized the interpretation of the results. The author participated in the electrochemical characterization and the interpretation of the results. Organized the writing process and finalized the manuscript for publication.

III. Atomic layer deposition of lithium nitride and carbonate using lithium silylamide

The author planned and performed the synthesis and characterization of all samples (except XPS), interpreted the results (except the results from Raman-spectroscopy), wrote and finalized the manuscript for publication. The DFT-calculations were performed by P. Vajeeston.

IV. Atomic layer deposition of ferroelectric $LiNbO_3$

The author planned the work together with Henrik Sønsteby and performed the synthesis, organized the experimental work and the interpretation of the results, except for the TOF-ERDA measurements and the PFM-measurements. The author organized the writing process and finalized the manuscript for publication.

V. Atomic Layer Deposition of Spinel Lithium Manganese Oxide for Thin Film Lithium Ion Batteries

The author participated in discussions to conceive the idea to the mechanism and design the experiments connected with ALD-growth, and performed all experiments with $Mn(EtCp)_2$ and contributed the manuscript.

VI. Atomic layer deposition of Sodium and Potassium oxides: Evaluation of precursors and deposition of thin films

The author conceived the idea and planned the work together with Henrik Sønsteby. Organized and conducted the synthesis and the experimental work and interpretation of the results, except solving the crystal structures. Organized the writing process and finalized the manuscript for publication.

VII. Epitaxial perovskites of sodium and potassium niobates by ALD (manuscript)

The author participated in discussions to conceive the idea and design the experiments and assisted in synthesis and characterization of the samples and participated in writing the manuscript.

7 References

1. *The Aviation Herald*. [cited 2013 26.11.2013]; 787-800 Battery Fire]. Available from: http://avherald.com/h?article=45c377c5&opt=0.
2. *Tesla Motors*. 26.11.2013]; Available from: 26.11.2013.
3. Tarascon, J.M. and M. Armand, *Issues and challenges facing rechargeable lithium batteries.* Nature (London, U. K.), 2001. **414**(6861): p. 359-367.
4. Flandrois, S. and B. Simon, *Carbon materials for lithium-ion rechargeable batteries.* Carbon, 1999. **37**(2): p. 165-180.
5. Reddy, M.V., R.G.V. Subba and B.V.R. Chowdari, *Metal Oxides and Oxysalts as Anode Materials for Li Ion Batteries.* Chem. Rev. (Washington, DC, U. S.), 2013. **113**(7): p. 5364-5457.
6. Nishijima, M., T. Kagohashi, Y. Takeda, M. Imanishi and O. Yamamoto, *Electrochemical studies of a new anode material, $Li_{3-x}M_xN$ (M = Co, Ni, Cu).* Journal of Power Sources, 1997. **68**(2): p. 510-514.
7. Li, H., Z. Wang, L. Chen and X. Huang, *Research on Advanced Materials for Li-ion Batteries.* Adv. Mater. (Weinheim, Ger.), 2009. **21**(45): p. 4593-4607.
8. Wang, Z., L. Zhou and X.W. Lou, *Metal Oxide Hollow Nanostructures for Lithium-ion Batteries.* Adv. Mater. (Weinheim, Ger.), 2012. **24**(14): p. 1903-1911.
9. Whittingham, M.S., *Electrical Energy Storage and Intercalation Chemistry.* Science, 1976. **192**(4244): p. 1126-1127.
10. Thackeray, M., *Lithium-ion batteries: An unexpected conductor.* Nat Mater, 2002. **1**(2): p. 81-82.
11. *IEEE Spectrum*. [cited 2013 26.11.13]; Available from: http://spectrum.ieee.org/green-tech/advanced-cars/lithium-batteries-take-to-the-road.
12. *A123 Systems*. [cited 2013 26.11.2013]; Available from: http://www.a123systems.com/lithium-battery.htm.
13. Kim, C., M. Noh, M. Choi, J. Cho and B. Park, *Critical Size of a Nano SnO_2 Electrode for Li-Secondary Battery.* Chemistry of Materials, 2005. **17**(12): p. 3297-3301.
14. Aravindan, V., J. Gnanaraj, S. Madhavi and H.-K. Liu, *Lithium-Ion Conducting Electrolyte Salts for Lithium Batteries.* Chemistry – A European Journal, 2011. **17**(51): p. 14326-14346.
15. Scrosati, B., J. Hassoun and Y.-K. Sun, *Lithium-ion batteries. A look into the future.* Energy & Environmental Science, 2011. **4**(9): p. 3287-3295.
16. Schaefer, J., Y. Lu, S. Moganty, P. Agarwal, N. Jayaprakash, and L. Archer, *Electrolytes for high-energy lithium batteries.* Applied Nanoscience, 2012. **2**(2): p. 91-109.
17. Scrosati, B. and J. Garche, *Lithium batteries: Status, prospects and future.* J. Power Sources, 2010. **195**(9): p. 2419-2430.
18. Goodenough, J.B. and Y. Kim, *Challenges for Rechargeable Li Batteries.* Chemistry of Materials, 2009.
19. Knauth, P., *Inorganic solid Li ion conductors: An overview.* Solid State Ionics, 2009. **180**(14–16): p. 911-916.
20. Goodenough, J.B. and K.-S. Park, *The Li-Ion Rechargeable Battery: A Perspective.* Journal of the American Chemical Society, 2013. **135**(4): p. 1167-1176.
21. Liu, J., M.N. Banis, X. Li, A. Lushington, M. Cai, R. Li, . . . X. Sun, *Atomic Layer Deposition of Lithium Tantalate Solid-State Electrolytes.* The Journal of Physical Chemistry C, 2013. **117**(39): p. 20260-20267.

22. Fergus, J.W., *Ceramic and polymeric solid electrolytes for lithium-ion batteries.* Journal of Power Sources, 2010. **195**(15): p. 4554-4569.
23. Zhou, Y.-N., M.-Z. Xue and Z.-W. Fu, *Nanostructured thin film electrodes for lithium storage and all-solid-state thin-film lithium batteries.* Journal of Power Sources, 2013. **234**(0): p. 310-332.
24. Glass, A.M., K. Nassau and T.J. Negran, *Ionic conductivity of quenched alkali niobate and tantalate glasses.* Journal of Applied Physics, 1978. **49**(9): p. 4808-4811.
25. Slater, M.D., D. Kim, E. Lee and C.S. Johnson, *Sodium-Ion Batteries.* Adv. Funct. Mater., 2013. **23**(8): p. 947-958.
26. Park, Y.-U., D.-H. Seo, H.-S. Kwon, B. Kim, J. Kim, H. Kim, . . . K. Kang, *A New High-Energy Cathode for a Na-Ion Battery with Ultrahigh Stability.* J. Am. Chem. Soc., 2013. **135**(37): p. 13870-13878.
27. Lu, X., G. Xia, J.P. Lemmon and Z. Yang, *Advanced materials for sodium-beta alumina batteries: Status, challenges and perspectives.* J. Power Sources, 2010. **195**(9): p. 2431-2442.
28. Xia, H., S.B. Tang and L. Lu, *Thin film microbatteries prepared by pulsed laser deposition.* J. Korean Phys. Soc., 2007. **51**(3): p. 1055-1062.
29. Notten, P.H.L., F. Roozeboom, R.A.H. Niessen and L. Baggetto, *3-D Integrated All-Solid-State Rechargeable Batteries.* Advanced Materials, 2007. **19**(24): p. 4564-4567.
30. Oudenhoven, J.F.M., L. Baggetto and P.H.L. Notten, *All-solid-state lithium-ion microbatteries: A review of various three-dimensional concepts.* Adv. Energy Mater., 2011. **1**(1): p. 10-33.
31. Bates, J.B., N.J. Dudney, B. Neudecker, A. Ueda and C.D. Evans, *Thin-film lithium and lithium-ion batteries.* Solid State Ionics, 2000. **135**(1-4): p. 33-45.
32. Oudenhoven, J.F.M., T. van Dongen, R.A.H. Niessen, M.H.J.M. de Croon and P.H.L. Notten, *Low-Pressure Chemical Vapor Deposition of $LiCoO_2$ Thin Films: A Systematic Investigation of the Deposition Parameters.* Journal of The Electrochemical Society, 2009. **156**(5): p. D169-D174.
33. Cho, S.-I. and S.-G. Yoon, *Characterization of $LiCoO_2$ thin film cathodes deposited by liquid-delivery metalorganic chemical vapor deposition for rechargeable lithium batteries.* J. Electrochem. Soc., 2002. **149**(12): p. A1584-A1588.
34. Julien, C., E. Haro-Poniatowski, M.A. Camacho-Lopez, L. Escobar-Alarcon and J. Jimenez-Jarquin, *Growth of V_2O_5 thin films by pulsed laser deposition and their applications in lithium microbatteries.* Mater. Sci. Eng., B, 1999. **B65**(3): p. 170-176.
35. Mantoux, A., H. Groult, E. Balnois, P. Doppelt and L. Gueroudji, *Vanadium Oxide Films Synthesized by CVD and Used as Positive Electrodes in Secondary Lithium Batteries.* J. Electrochem. Soc., 2004. **151**(3): p. A368-A373.
36. McGraw, J.M., J.D. Perkins, J.G. Zhang, P. Liu, P.A. Parilla, J. Turner, . . . D.S. Ginley, *Next generation V_2O_5 cathode materials for Li rechargeable batteries.* Solid State Ionics, 1998. **113-115**: p. 407-413.
37. Whitacre, J.F., W.C. West, E. Brandon and B.V. Ratnakumar, *Crystallographically Oriented Thin-Film Nanocrystalline Cathode Layers Prepared Without Exceeding 300°C.* Journal of The Electrochemical Society, 2001. **148**(10): p. A1078-A1084.
38. *Infinite power solutions*. [cited 2013 16.12.13]; Available from: http://www.cytech.com/products-ips;jsessionid=D133123504964A6E9CA39F3574C3746B.
39. *EnerChip*. [cited 2013 16.12.13]; Available from: http://www.cymbet.com/products/enerchip-overview.php.

40. *Excellatron*. [cited 2013 16.12.13]; Available from: http://www.excellatron.com/advantage.htm.
41. Long, J.W., B. Dunn, D.R. Rolison and H.S. White, *Three-Dimensional Battery Architectures.* Chemical Reviews, 2004. **104**(10): p. 4463-4492.
42. *EnerChip White Paper: Design Advantages of Solid State Batteries vs. Supercapacitors* Available from: http://www.cymbet.com/pdfs/WP-EnerChips-vs-Supercaps.pdf.
43. Takada, K., H. Sakurai, E. Takayama-Muromachi, F. Izumi, R.A. Dilanian, and T. Sasaki, *Superconductivity in two-dimensional CoO_2 layers.* Nature, 2003. **422**(6927): p. 53-55.
44. Brinks, P., H. Heijmerikx, T.A. Hendriks, G. Rijnders and M. Huijben, *Achieving chemical stability in thermoelectric Na_xCoO_2 thin films.* RSC Adv., 2012. **2**(14): p. 6023-6027.
45. Son, J.Y., Y.H. Shin and C.S. Park, *Enhanced power factor of epitaxial layered cobaltite Na_xCoO_2 thin film induced by strain: x=0.5,0.7.* J. Appl. Phys., 2008. **104**(3): p. 033538/1-033538/4.
46. Muralt, P., *Ferroelectric thin films for micro-sensors and actuators: a review.* Journal of Micromechanics and Microengineering, 2000. **10**(2): p. 136.
47. Paul, M., *Micromachined infrared detectors based on pyroelectric thin films.* Reports on Progress in Physics, 2001. **64**(10): p. 1339.
48. Christen, H.M., L.A. Boatner, J.D. Budai, M.F. Chisholm, L.A. Gea, P.J. Marrero, and D.P. Norton, *The growth and properties of epitaxial $KNbO_3$ thin films and $KNbO_3/KTaO_3$ superlattices.* Appl. Phys. Lett., 1996. **68**(11): p. 1488-90.
49. Romanov, M.V., I.E. Korsakov, A.R. Kaul, S.Y. Stefanovich, I.A. Bolshakov, and G. Wahl, *MOCVD of $KNbO_3$ ferroelectric films and their characterization.* Chem. Vap. Deposition, 2004. **10**(6): p. 318-324.
50. Saito, T., T. Wada, H. Adachi and I. Kanno, *Epitaxial growth of (K,Na)NbO_3 thin films deposited on (100)$SrTiO_3$ substrate by PLD.* Nippon Kessho Seicho Gakkaishi, 2004. **31**(3): p. 234.
51. Saito, T., H. Adachi, T. Wada and H. Adachi, *Pulsed-laser deposition of ferroelectric $NaNbO_3$ thin films.* Jpn. J. Appl. Phys., Part 1, 2005. **44**(9B): p. 6969-6972.
52. Savage, A., *Pyroelectricity and spontaneous polarization in $LiNbO_3$.* J. Appl. Phys., 1966. **37**: p. 3071-2.
53. Wang, H.F., Y.Y. Zhu, S.N. Zhu and N.B. Ming, *Investigation of ferroelectric coercive field in $LiNbO_3$.* Applied Physics A: Materials Science & Processing, 1997. **65**(4): p. 437-438.
54. Inbar, I. and R.E. Cohen, *Origin of ferroelectricity in $LiNbO_3$ and $LiTaO_3$.* Ferroelectrics, 1997. **194**(1): p. 83-95.
55. Han, S.-T., Y. Zhou and V.A.L. Roy, *Towards the Development of Flexible Non-volatile Memories.* Adv. Mater. (Weinheim, Ger.), 2013. **25**(38): p. 5425-5449.
56. Arimoto, Y. and H. Ishiwara, *Current status of ferroelectric random-access memory.* MRS Bull., 2004. **29**: p. 823-828.
57. Suntola, T., *Atomic layer epitaxy.* Thin Solid Films, 1992. **216**(1): p. 84-89.
58. *ASM Pulsar 3000*. 2013 [cited 2013 24.11.2013]; Available from: http://www.asmtheswitchison.com/pulsarPage.php.
59. Li, W.-M., *Recent Developments of Atomic Layer Deposition Processes for Metallization.* Chemical Vapor Deposition, 2013. **19**(4-6): p. 82-103.
60. Puurunen, R.L., H. Kattelus and T. Suntola. *Atomic layer deposition in MEMS technology*. 2010. Elsevier Ltd.

61. Puurunen, R.L., J. Saarilahti and H. Kattelus, *Implementing ALD layers in MEMS processing.* ECS Trans., 2007. **11**(7, Atomic Layer Deposition Applications 3): p. 3-14.
62. Jylhä, O., M. Putkonen and A. Pakkala, *Fabrication of strengthened structural module for optical display devices*. 2012, Beneq Oy, Finland . p. 29 pp.
63. Hirvikorpi, T., M. Vähä-Nissi, A. Harlin and M. Karppinen, *Comparison of some coating techniques to fabricate barrier layers on packaging materials.* Thin Solid Films, 2010. **518**(19): p. 5463-5466.
64. Hirvikorpi, T., M. Vähä-Nissi, A. Harlin, J. Marles, V. Miikkulainen, and M. Karppinen, *Effect of corona pre-treatment on the performance of gas barrier layers applied by atomic layer deposition onto polymer-coated paperboard.* Appl. Surf. Sci., 2010. **257**(3): p. 736-740.
65. Hirvikorpi, T., R. Laine, M. Vaha-Nissi, V. Kilpi, E. Salo, W.-M. Li, . . . J. Kostamo, *Barrier properties of plastic films coated with an Al_2O_3 layer by roll-to-toll atomic layer deposition.* Thin Solid Films: p. Ahead of Print.
66. Härköenen, E., B. Diaz, J. Swiatowska, V. Maurice, A. Seyeux, M. Fenker, . . . M. Ritala, *$Al_xTa_yO_z$ Mixture Coatings Prepared Using Atomic Layer Deposition for Corrosion Protection of Steel.* Chem. Vap. Deposition, 2013. **19**(4-5-6): p. 194-203.
67. Marin, E., A. Lanzutti, M. Lekka, L. Guzman, W. Ensinger, and L. Fedrizzi, *Chemical and mechanical characterization of TiO_2/Al_2O_3 atomic layer depositions on AISI 316 L stainless steel.* Surf. Coat. Technol., 2012. **211**: p. 84-88.
68. Ferguson, J.D., A.W. Weimer and S.M. George, *Atomic layer deposition of Al_2O_3 films on polyethylene particles.* Chem. Mater., 2004. **16**(26): p. 5602-5609.
69. Ott, A.W. and R.P.H. Chang, *Atomic layer-controlled growth of transparent conducting ZnO on plastic substrates.* Mater. Chem. Phys., 1999. **58**(2): p. 132-138.
70. Aaltonen, T., P. Alen, M. Ritala and M. Leskelä, *Ruthenium thin films grown by atomic layer deposition.* Chem. Vap. Deposition, 2003. **9**(1): p. 45-49.
71. Aaltonen, T., M. Ritala, T. Sajavaara, J. Keinonen and M. Leskelä, *Atomic Layer Deposition of Platinum Thin Films.* Chem. Mater., 2003. **15**(9): p. 1924-1928.
72. Im, H., N.J. Wittenberg, N.C. Lindquist and S.-H. Oh, *Atomic layer deposition: a versatile technique for plasmonics and nanobiotechnology.* J. Mater. Res., 2012. **27**(4): p. 663-671.
73. Elam, J.W., C.E. Nelson, R.K. Grubbs and S.M. George, *Kinetics of the WF_6 and Si_2H_6 surface reactions during tungsten atomic layer deposition.* Surf. Sci., 2001. **479**(1-3): p. 121-135.
74. Pore, V., K. Knapas, T. Hatanpää, T. Sarnet, M. Kemell, M. Ritala, . . . K. Mizohata, *Atomic Layer Deposition of Antimony and its Compounds Using Dechlorosilylation Reactions of Tris(triethylsilyl)antimony.* Chem. Mater., 2011. **23**(2): p. 247-254.
75. Pessa, M., R. Makela and T. Suntola, *Characterization of surface exchange reactions used to grow compound films.* Appl. Phys. Lett., 1981. **38**(3): p. 131-2.
76. Oya, G., M. Yoshida and Y. Sawada, *Growth of α-alumina films by molecular layer epitaxy.* Appl. Phys. Lett., 1987. **51**(15): p. 1143-5.
77. Hiltunen, L., H. Kattelus, M. Leskelä, M. Mäkelä, L. Niinistö, E. Nykänen, . . . M. Tiitta, *Growth and characterization of aluminum oxide thin films deposited from various source materials by atomic layer epitaxy and chemical vapor deposition processes.* Mater. Chem. Phys., 1991. **28**(4): p. 379-88.
78. Aarik, J., A. Aidla, K. Kukli and T. Uustare, *Deposition and etching of tantalum oxide films in atomic layer epitaxy process.* J. Cryst. Growth, 1994. **144**(1/2): p. 116-19.

79. Hiltunen, L., M. Leskelä, M. Makela, L. Niinistö, E. Nykanen, and P. Soininen, *Nitrides of titanium, niobium, tantalum and molybdenum grown as thin films by the atomic layer epitaxy method.* Thin Solid Films, 1988. **166**: p. 149-54.
80. Østreng, E., P. Vajeeston, O. Nilsen and H. Fjellvåg, *Atomic layer deposition of lithium nitride and carbonate using lithium silylamide.* RSC Advances, 2012. **2**(15): p. 6315-6322.
81. Ritala, M., M. Leskelä, E. Rauhala and P. Haussalo, *Atomic layer epitaxy growth of TiN thin films.* J. Electrochem. Soc., 1995. **142**(8): p. 2731-7.
82. Kidder, J.N., Jr., H.K. Yun, J.W. Rogers and T.P. Pearsall, *Chemical Composition of AlN Thin Films Deposited at 523-723 K Using Dimethylethylamine Alane and Ammonia.* Chem. Mater., 1998. **10**(3): p. 777-783.
83. Ritala, M., M. Leskelä, E. Rauhala and J. Jokinen, *Atomic layer epitaxy growth of TiN thin films from TiI_4 and NH_3.* J. Electrochem. Soc., 1998. **145**(8): p. 2914-2920.
84. Ritala, M., T. Asikainen, M. Leskelä, J. Jokinen, R. Lappalainen, M. Utriainen, . . . E. Ristolainen, *Effects of intermediate zinc pulses on properties of TiN and NbN films deposited by atomic layer epitaxy.* Appl. Surf. Sci., 1997. **120**(3/4): p. 199-212.
85. Putkonen, M., T. Sajavaara, P. Rahkila, L. Xu, S. Cheng, L. Niinistoe, and H.J. Whitlow, *Atomic layer deposition and characterization of biocompatible hydroxyapatite thin films.* Thin Solid Films, 2009. **517**(20): p. 5819-5824.
86. Hämäläinen, J., J. Holopainen, F. Munnik, T. Hatanpää, M. Heikkilä, M. Ritala, and M. Leskelä, *Lithium Phosphate Thin Films Grown by Atomic Layer Deposition.* J. Electrochem. Soc., 2012. **159**(3): p. A259-A263.
87. Hämäläinen, J., J. Holopainen, F. Munnik, M. Heikkilä, M. Ritala, and M. Leskelä, *Atomic Layer Deposition of Aluminum and Titanium Phosphates.* J. Phys. Chem. C, 2012. **116**(9): p. 5920-5925.
88. Proslier, T., J.A. Klug, J.W. Elam, H. Claus, N.G. Becker, and M.J. Pellin, *Atomic Layer Deposition and Superconducting Properties of NbSi Films.* J. Phys. Chem. C, 2011. **115**(19): p. 9477-9485.
89. Klug, J.A., T. Proslier, J.W. Elam, R.E. Cook, J.M. Hiller, H. Claus, . . . M.J. Pellin, *Atomic layer deposition of amorphous niobium carbide-based thin film superconductors.* J. Phys. Chem. C, 2011. **115**(50): p. 25063-25071.
90. Martinson, A.B.F., J.W. Elam and M.J. Pellin, *Atomic layer deposition of Cu_2S for future application in photovoltaics.* Appl. Phys. Lett., 2009. **94**(12): p. 123107/1-123107/3.
91. Tornqvist, R. and S. Korpela, *On the aging of manganese-doped zinc sulfide electroluminescent thin films grown by the atomic-layer epitaxy technique.* J. Cryst. Growth, 1982. **59**(1-2): p. 395-8.
92. Ihanus, J., T. Hänninen, T. Hatanpää, T. Aaltonen, I. Mutikainen, T. Sajavaara, . . . M. Leskelä, *Atomic Layer Deposition of SrS and BaS Thin Films Using Cyclopentadienyl Precursors.* Chem. Mater., 2002. **14**(5): p. 1937-1944.
93. Pore, V., T. Hatanpää, M. Ritala and M. Leskelä, *Atomic Layer Deposition of Metal Tellurides and Selenides Using Alkylsilyl Compounds of Tellurium and Selenium.* J. Am. Chem. Soc., 2009. **131**(10): p. 3478-3480.
94. Sarnet, T., V. Pore, T. Hatanpää, M. Ritala, M. Leskelä, A. Schrott, . . . H.-Y. Cheng, *Atomic Layer Deposition and Characterization of GeTe Thin Films.* J. Electrochem. Soc., 2011. **158**(12): p. D694-D697.
95. Pilvi, T., T. Hatanpää, E. Puukilainen, K. Arstila, M. Bischoff, U. Kaiser, . . . M. Ritala, *Study of a novel ALD process for depositing MgF_2 thin films.* J. Mater. Chem., 2007. **17**(48): p. 5077-5083.

96. Pilvi, T., E. Puukilainen, K. Arstila, M. Leskelä and M. Ritala, *Atomic layer deposition of LaF_3 thin films using $La(thd)_3$ and TiF_4 as precursors.* Chem. Vap. Deposition, 2008. **14**(3-4): p. 85-91.
97. Pilvi, T., E. Puukilainen, U. Kreissig, M. Leskelä and M. Ritala, *Atomic Layer Deposition of MgF_2 Thin Films Using TaF_5 as a Novel Fluorine Source.* Chem. Mater., 2008. **20**(15): p. 5023-5028.
98. Mäntymäki, M., J. Hämäläinen, E. Puukilainen, F. Munnik, M. Ritala, and M. Leskelä, *Atomic Layer Deposition of LiF Thin Films from Lithd and TiF_4 Precursors.* Chemical Vapor Deposition, 2013. **19**(4-6): p. 111-116.
99. Mäntymäki, M., J. Hämäläinen, E. Puukilainen, T. Sajavaara, M. Ritala, and M. Leskelä, *Atomic Layer Deposition of LiF Thin Films from Lithd, $Mg(thd)_2$, and TiF_4 Precursors.* Chemistry of Materials, 2013. **25**(9): p. 1656-1663.
100. Ylilammi, M. and T. Ranta-aho, *Metal fluoride thin films prepared by atomic layer deposition.* J. Electrochem. Soc., 1994. **141**(5): p. 1278-84.
101. Miikkulainen, V., M. Leskelä, M. Ritala and R.L. Puurunen, *Crystallinity of inorganic films grown by atomic layer deposition: Overview and general trends.* Journal of Applied Physics, 2013. **113**(2): p. 021301-101.
102. Klepper, K.B., O. Nilsen and H. Fjellvåg, *Epitaxial growth of cobalt oxide by atomic layer deposition.* J. Cryst. Growth, 2007. **307**(2): p. 457-465.
103. Østreng, E., O. Nilsen and H. Fjellvåg, *Optical Properties of Vanadium Pentoxide Deposited by ALD.* The Journal of Physical Chemistry C, 2012. **116**(36): p. 19444-19450.
104. Østreng, E., H. Sønsteby, T. Sajavaara, O. Nilsen and H. Fjellvåg, *Atomic Layer Deposition of Ferroelectric $LiNbO_3$.* J. Mater. Chem. C, 2013. **1**: p. 4283-4290.
105. Nilsen, O., H. Fjellvåg and A. Kjekshus, *Growth of manganese oxide thin films by atomic layer deposition.* Thin Solid Films, 2003. **444**(1–2): p. 44-51.
106. Nilsen, O., H. Fjellvåg and A. Kjekshus, *Growth of calcium carbonate by the atomic layer chemical vapour deposition technique.* Thin Solid Films, 2004. **450**(2): p. 240-247.
107. Nilsen, O., E. Rauwel, H. Fjellvåg and A. Kjekshus, *Growth of $La_{1-x}Ca_xMnO_3$ thin films by atomic layer deposition.* J. Mater. Chem., 2007. **17**(15): p. 1466-1475.
108. Sønsteby, H.H., E. Østreng, H. Fjellvåg and O. Nilsen, *Deposition and x-ray characterization of epitaxial thin films of $LaAlO_3$.* Thin Solid Films, 2014. **550**(0): p. 90-94.
109. Nilsen, O., M. Lie, S. Foss, H. Fjellvåg and A. Kjekshus, *Effect of magnetic field on the growth of α-Fe_2O_3 thin films by atomic layer deposition.* Applied Surface Science, 2004. **227**(1–4): p. 40-47.
110. Lie, M., H. Fjellvåg and A. Kjekshus, *Growth of Fe_2O_3 thin films by atomic layer deposition.* Thin Solid Films, 2005. **488**(1-2): p. 74-81.
111. Zhang, F., G. Sun, W. Zhao, L. Wang, L. Zheng, S. Liu, . . . Y. Zeng, *Atomic Layer Deposition of $BiFeO_3$ Thin Films Using β-Diketonates and H_2O.* The Journal of Physical Chemistry C, 2013. **117**(46): p. 24579-24585.
112. Kessels, W.M.M. and M. Putkonen, *Advanced process technologies: plasma, direct-write, atmospheric pressure, and roll-to-roll ALD.* MRS Bull., 2011. **36**(11): p. 907-913.
113. Ritala, M. and M. Leskelä. *Atomic layer deposition*. 2002. Academic Press.
114. Ericsson, P., S. Bengtsson and J. Skarp, *Properties of Al_2O_3-films deposited on silicon by atomic layer epitaxy.* Microelectron. Eng., 1997. **36**(1-4): p. 91-94.

115. Aarik, J., A. Aidla, H. Mandar, V. Sammelselg and T. Uustare, *Texture development in nanocrystalline hafnium dioxide thin films grown by atomic layer deposition.* J. Cryst. Growth, 2000. **220**(1-2): p. 105-113.
116. Aarik, J., A. Aidla, H. Mandar and T. Uustare, *Atomic layer deposition of titanium dioxide from $TiCl_4$ and H_2O. Investigation of growth mechanism.* Appl. Surf. Sci., 2001. **172**(1-2): p. 148-158.
117. Lie, M., O. Nilsen, H. Fjellvåg and A. Kjekshus, *Growth of $La_{1-x}Sr_xFeO_3$ thin films by atomic layer deposition.* Dalton Trans., 2009(3): p. 481-489.
118. Elliott, S.D. and O. Nilsen, *(Invited) Reaction Mechanisms in ALD of Ternary Oxides.* ECS Transactions, 2011. **41**(2): p. 175-183.
119. *Beneq TFS NX300*. 2013 24.11.2013]; Available from: http://www.beneq.com/tfs-nx300.html.
120. *Picosun P1000*. 2013 [cited 2013 24.11.2013]; Available from: http://www.picosun.com/en/products/picosun8482+p-series/p-1000+technical+data+sheet/.
121. *Picosun PicoBatch*. 2013 [cited 2013 24.11.2013]; Available from: http://www.picosun.com/en/products/picobatch8482+ald+system/.
122. Elam, J.W., *Coatings on High Aspect Ratio Structures*, in *Atomic Layer Deposition of Nanostructured Materials*, M. Knez and N. Pinna, Editors. 2012, Wiley VCH Verlag GmbH. p. 227-249.
123. Meng, X., X.-Q. Yang and X. Sun, *Emerging Applications of Atomic Layer Deposition for Lithium-Ion Battery Studies.* Adv. Mater. (Weinheim, Ger.), 2012. **24**(27): p. 3589-3615.
124. Jung, Y.S., A.S. Cavanagh, L.A. Riley, S.-H. Kang, A.C. Dillon, M.D. Groner, . . . S.-H. Lee, *Ultrathin Direct Atomic Layer Deposition on Composite Electrodes for Highly Durable and Safe Li-Ion Batteries.* Adv. Mater. (Weinheim, Ger.), 2010. **22**(19): p. 2172-2176.
125. Miikkulainen, V., A. Ruud, E. Østreng, O. Nilsen, M. Laitinen, T. Sajavaara, and H. Fjellvåg, *Atomic Layer Deposition of Spinel Lithium Manganese Oxide via Film Body Controlled*
Lithium Incorporation for Thin Film Lithium Ion Batteries. Journal of Physical Chemistry C, 2013. **Submitted**.
126. Miikkulainen, V., O. Nilsen, M. Laitinen, T. Sajavaara and H. Fjellvåg, *Atomic layer deposition of $Li_xTi_yO_z$ thin films.* RSC Advances, 2013. **3**(20): p. 7537-7542.
127. Aaltonen, T., M. Alnes, O. Nilsen, L. Costelle and H. Fjellvåg, *Lanthanum titanate and lithium lanthanum titanate thin films grown by atomic layer deposition.* J. Mater. Chem., 2010. **20**(14): p. 2877-2881.
128. Aaltonen, T., O. Nilsen, A. Magraso and H. Fjellvåg, *Atomic Layer Deposition of Li_2O-Al_2O_3 Thin Films.* Chem. Mater., 2011. **23**(11): p. 4669-4675.
129. Chen, Z., Y. Qin, K. Amine and Y.K. Sun, *Role of surface coating on cathode materials for lithium-ion batteries.* J. Mater. Chem., 2010. **20**(36): p. 7606-7612.
130. Donders, M.E., W.M. Arnoldbik, H.C.M. Knoops, W.M.M. Kessels and P.H.L. Notten, *Atomic Layer Deposition of $LiCoO_2$ Thin-Film Electrodes for All-Solid-State Li-Ion Micro-Batteries.* Journal of The Electrochemical Society, 2013. **160**(5): p. A3066-A3071.
131. Le, V.K., H. Groult, A. Mantoux, L. Perrigaud, F. Lantelme, R. Lindstroem, . . . D. Lincot, *Amorphous vanadium oxide films synthesised by ALCVD for lithium rechargeable batteries.* J. Power Sources, 2006. **160**(1): p. 592-601.

132. Badot, J.C., A. Mantoux, N. Baffier, O. Dubrunfaut and D. Lincot, *Submicro- and nanostructural effects on electrical properties of $Li_{0.2}V_2O_5$ thin films obtained by atomic layer deposition (ALD).* J. Phys. Chem. Solids, 2006. **67**(5-6): p. 1270-1274.
133. Badot, J.C., A. Mantoux, N. Baffier, O. Dubrunfaut and D. Lincot, *Electrical properties of V_2O_5 thin films obtained by atomic layer deposition (ALD).* J. Mater. Chem., 2004. **14**(23): p. 3411-3415.
134. Chen, X., E. Pomerantseva, P. Banerjee, K. Gregorczyk, R. Ghodssi, and G. Rubloff, *Ozone-Based Atomic Layer Deposition of Crystalline V_2O_5 Films for High Performance Electrochemical Energy Storage.* Chem. Mater., 2012. **24**(7): p. 1255-1261.
135. Chen, X., E. Pomerantseva, K. Gregorczyk, R. Ghodssi and G. Rubloff, *Cathodic ALD V_2O_5 thin films for high-rate electrochemical energy storage.* RSC Adv., 2013. **3**(13): p. 4294-4302.
136. Chen, X., H. Zhu, Y.-C. Chen, Y. Shang, A. Cao, L. Hu, and G.W. Rubloff, *MWCNT/V_2O_5 Core/Shell Sponge for High Areal Capacity and Power Density Li-Ion Cathodes.* ACS Nano, 2012. **6**(9): p. 7948-7955.
137. Pomerantseva, E., K. Gerasopoulos, X. Chen, G. Rubloff and R. Ghodssi, *Electrochemical performance of the nanostructured biotemplated V_2O_5 cathode for lithium-ion batteries.* Journal of Power Sources, 2012. **206**(0): p. 282-287.
138. Meng, X., J. Liu, X. Li, M.N. Banis, J. Yang, R. Li, and X. Sun, *Atomic layer deposited $Li_4Ti_5O_{12}$ on nitrogen-doped carbon nanotubes.* RSC Advances, 2013. **3**(20): p. 7285-7288.
139. Aravindan, V., K.B. Jinesh, R.R. Prabhakar, V.S. Kale and S. Madhavi, *Atomic layer deposited (ALD) SnO_2 anodes with exceptional cycleability for Li-ion batteries.* Nano Energy, 2013. **2**(5): p. 720-725.
140. Panda, S.K., Y. Yoon, H.S. Jung, W.-S. Yoon and H. Shin, *Nanoscale size effect of titania (anatase) nanotubes with uniform wall thickness as high performance anode for lithium-ion secondary battery.* J. Power Sources, 2012. **204**: p. 162-167.
141. Leung, K., Y. Qi, K.R. Zavadil, Y.S. Jung, A.C. Dillon, A.S. Cavanagh, . . . S.M. George, *Using Atomic Layer Deposition to Hinder Solvent Decomposition in Lithium Ion Batteries: First-Principles Modeling and Experimental Studies.* J. Am. Chem. Soc., 2011. **133**(37): p. 14741-14754.
142. Jung, Y.S., A.S. Cavanagh, A.C. Dillon, M.D. Groner, S.M. George, and S.-H. Lee, *Enhanced Stability of $LiCoO_2$ Cathodes in Lithium-Ion Batteries Using Surface Modification by Atomic Layer Deposition.* J. Electrochem. Soc., 2010. **157**(1): p. A75-A81.
143. Guan, D., J.A. Jeevarajan and Y. Wang, *Enhanced cycleability of $LiMn_2O_4$ cathodes by atomic layer deposition of nanosized-thin Al_2O_3 coatings.* Nanoscale, 2011. **3**(4): p. 1465-1469.
144. Jung, Y.S., A.S. Cavanagh, Y. Yan, S.M. George and A. Manthiram, *Effects of atomic layer deposition of Al_2O_3 on the $Li[Li_{0.2}Mn_{0.54}Ni_{0.13}Co_{0.13}]O_2$ cathode for lithium-ion batteries.* J. Electrochem. Soc., 2011. **158**(12): p. A1298-A1302.
145. Snyder, M.Q., S. Trebukhova, B. Ravdel, M.C. Wheeler, J. DiCarlo, C.P. Tripp, and S.W.J. De, *Preparation and Characterization of ALD TiN Thin Films on Lithium Titanate Spinel ($Li_4Ti_5O_{12}$) for Lithium Ion Battery Applications.* Mater. Res. Soc. Symp. Proc., 2007. **973E**(Mobile Energy): p. No pp. given, Paper #: 0972-AA07-05-BB08-05.

146. Li, X., J. Liu, X. Meng, Y. Tang, M.N. Banis, J. Yang, . . . X. Sun, *Significant impact on cathode performance of lithium-ion batteries by precisely controlled metal oxide nanocoatings via atomic layer deposition.* J. Power Sources, 2014. **247**: p. 57-69.
147. Nilsen, O., V. Miikkulainen, K.B. Gandrud, E. Østreng, A. Ruud, and H. Fjellvåg, *Atomic layer deposition of functional films for Li-ion microbatteries.* Physica Status Solidi, 2013.
148. Putkonen, M., T. Aaltonen, M. Alnes, T. Sajavaara, O. Nilsen, and H. Fjellvåg, *Atomic layer deposition of lithium containing thin films.* J. Mater. Chem., 2009. **19**(46): p. 8767-8771.
149. Liu, J., M.N. Banis, X. Li, A. Lushington, M. Cai, R. Li, . . . X. Sun, *Atomic Layer Deposition of Lithium Tantalate Solid-State Electrolytes.* J. Phys. Chem. C, 2013. **117**(39): p. 20260-20267.
150. Hämäläinen, J., F. Munnik, T. Hatanpää, J. Holopainen, M. Ritala, and M. Leskela, *Study of amorphous lithium silicate thin films grown by atomic layer deposition.* Journal of Vacuum Science & Technology A: Vacuum, Surfaces, and Films, 2012. **30**(1): p. 01A106-1-5.
151. Wannagat, U., *N-metallated silicon-nitrogen derivatives: preparation, structure and reactions.* Pure and Applied Chemistry, 1969. **19**(3-4): p. 329-342.
152. Fjeldberg, T., M.F. Lappert and A.J. Thorne, *The molecular structure of dimeric bis(trimethylsilyl)amidolithium, [LiN(Si(CH$_3$)$_3$)$_2$]$_2$, as determined by gas-phase electron diffraction.* Journal of Molecular Structure, 1984. **125**(3-4): p. 265-275.
153. Nekola, H., F. Olbrich and U. Behrens, *Kristall- und Molekülstrukturen von Lithium- und Natrium-tert-butoxid.* Zeitschrift für anorganische und allgemeine Chemie, 2002. **628**(9-10): p. 2067-2070.
154. Hartwell, G.E. and T.L. Brown, *The Mass Spectra of Lithiomethyltrimethylsilane and Lithium t-Butoxide.* Inorganic Chemistry, 1966. **5**(7): p. 1257-1259.
155. Kahn, J.D., A. Haag and P.v.R. Schleyer, *Mass spectrometry of gas-phase lithium alkoxides.* The Journal of Physical Chemistry, 1988. **92**(1): p. 212-220.
156. Filatov, E.S., S.V. Sysoev, L.N. Zelenina, T.P. Chusova, V.A. Logvinenko, P.P. Semyannikov, and I.K. Igumenov, *Thermodynamic study of a series lithium β-diketonates.* J. Therm. Anal. Calorim., 2006. **86**(2): p. 537-539.
157. Gillan, E.G., S.G. Bott and A.R. Barron, *Volatility Studies on Gallium Chalcogenide Cubanes: Thermal Analysis and Determination of Sublimation Enthalpies.* Chemistry of Materials, 1997. **9**(3): p. 796-806.
158. Nieminen, M., M. Putkonen and L. Niinistö, *Formation and stability of lanthanum oxide thin films deposited from β-diketonate precursor.* Appl. Surf. Sci., 2001. **174**(2): p. 155-166.
159. Tabassum, S., O. Sereda, P.V.G. Reddy and R. Wilhelm, *Hindered Bronsted bases as Lewis base catalysts.* Organic & Biomolecular Chemistry, 2009. **7**(19): p. 4009-4016.
160. Bunting, J.W., J.P. Kanter, R. Nelander and Z. Wu, *The acidity and tautomerism of β-diketones in aqueous solution.* Canadian Journal of Chemistry, 1995. **73**(8): p. 1305-1311.
161. Grüning, R. and J.L. Atwood, *The crystal structure of N-sodiohexamethyldisilazane, Na[N{Si(CH$_3$)$_3$}$_2$].* Journal of Organometallic Chemistry, 1977. **137**(1): p. 101-111.
162. Green, J.C., M. Payne, E.A. Seddon and R.A. Andersen, *He-I and He-II photoelectron studies of bonding in metal silylamido-complexes, M[N(SiMe$_3$)$_2$](n= 1,2, or 3).* Journal of the Chemical Society, Dalton Transactions, 1982(5): p. 887-892.

163. Tesh, K.F., T.P. Hanusa and J.C. Huffman, *Ion pairing in [bis(trimethylsilyl)amido]potassium: The x-ray crystal structure of unsolvated [KN(SiMe$_3$)$_2$]$_2$.* Inorganic Chemistry, 1990. **29**(8): p. 1584-1586.
164. Østreng, E., H.H. Sønsteby, S. Øien, O. Nilsen and H. Fjellvåg, *Atomic Layer Deposition of Sodium and Potassium Oxides: Evaluation of Precursors and Deposition of Thin Films.* Dalton Transactions, 2014.
165. Weiss, E., K. Hoffmann and H.-F. Gr ützmacher, *Röntgenographische und massenspektrometrische Untersuchung der Alkalitrimethylasilanolate.* Chemische Berichte, 1970. **103**(4): p. 1190-1197.
166. Chisholm, M.H., S.R. Drake, A.A. Naiini and W.E. Streib, *Synthesis and X-ray crystal structures of the one-dimensional ribbon chains [MOBut·ButOH]∞ and the cubane species [MOBut]$_4$ (M = K and Rb).* Polyhedron, 1991. **10**(3): p. 337-345.
167. Greiser, T. and E. Weiss, *Crystal structure of sodium tert-butoxide, [(CH$_3$)$_3$CONa]$_9$.[(CH$_3$)$_3$CONa]$_6$, a new type of structure with nonameric and hexameric units.* Chem. Ber., 1977. **110**(10): p. 3388-96.
168. Weiss, E., H. Alsdorf, H. Kühr and H.-F. Grützmacher, *Röntgenographische, NMR- und massenspektrometrische Untersuchungen der tert.-Butylate des Kaliums, Rubidiums und Cäsiums.* Chemische Berichte, 1968. **101**(11): p. 3777-3786.
169. Saulys, D., V. Joshkin, M. Khoudiakov, T.F. Kuech, A.B. Ellis, S.R. Oktyabrsky, and L. McCaughan, *An examination of the surface decomposition chemistry of lithium niobate precursors under high vacuum conditions.* Journal of Crystal Growth, 2000. **217**(3): p. 287-301.
170. Heitjans, P. and S. Indris, *Diffusion and ionic conduction in nanocrystalline ceramics.* J. Phys.: Condens. Matter, 2003. **15**(30): p. R1257-R1289.
171. Sebastian, L. and J. Gopalakrishnan, *Lithium ion mobility in metal oxides: A materials chemistry perspective.* J. Mater. Chem., 2003. **13**(3): p. 433-441.
172. Kosola, A., M. Putkonen, L.-S. Johansson and L. Niinistö, *Effect of annealing in processing of strontium titanate thin films by ALD.* Appl. Surf. Sci., 2003. **211**(1-4): p. 102-112.
173. Vehkamäki, M., T. Hanninen, M. Ritala, M. Leskelä, T. Sajavaara, E. Rauhala, and J. Keinonen, *Atomic layer deposition of SrTiO$_3$ thin films from a novel strontium precursor - strontium bis(tri-isopropylcyclopentadienyl).* Chem. Vap. Deposition, 2001. **7**(2): p. 75-80.
174. Vehkamäki, M., T. Hatanpää, M. Ritala, M. Leskelä, S. Vayrynen, and E. Rauhala, *Atomic layer deposition of BaTiO$_3$ thin films - effect of barium hydroxide formation.* Chem. Vap. Deposition, 2007. **13**(5): p. 239-246.
175. Päiväsaari, J., M. Putkonen and L. Niinistö, *A comparative study on lanthanide oxide thin films grown by atomic layer deposition.* Thin Solid Films, 2005. **472**(1-2): p. 275-281.
176. Comstock, D.J. and J.W. Elam, *Mechanistic Study of Lithium Aluminum Oxide Atomic Layer Deposition.* The Journal of Physical Chemistry C, 2012. **117**(4): p. 1677-1683.
177. Cavanagh, A.S., Y. Lee, B. Yoon and S. George, *Atomic Layer Deposition of LiOH and Li$_2$CO$_3$ Using Lithium t-Butoxide as the Lithium Source.* ECS Transactions, 2010. **33**(2): p. 223-229.
178. Østreng, E., P. Vajeeston, O. Nilsen and H. Fjellvåg, *Atomic layer deposition of lithium nitride and carbonate using lithium silylamide.* RSC Adv., 2012. **2**(15): p. 6315-6322.
179. Tomczak, Y., K. Knapas, M. Sundberg, M. Leskelä and M. Ritala, *In Situ Reaction Mechanism Studies on Lithium Hexadimethyldisilazide and Ozone Atomic Layer*

Deposition Process for Lithium Silicate. J. Phys. Chem. C, 2013. **117**(27): p. 14241-14246.
180. Zhang, H., Z. Wang and J. Dai, *A study of the thermodynamic properties and dehydration reaction kinetics of some salt-hydrates.* Journal of thermal analysis, 1995. **45**(1-2): p. 109-115.
181. Parratt, L.G., *Surface Studies of Solids by Total Reflection of X-Rays.* Physical Review, 1954. **95**(2): p. 359-369.
182. *J.A Woollam*. 2013 [cited 2013 22 Nov]; Available from: http://www.jawoollam.com/tutorial_4.html.
183. Johs, B. and J.S. Hale, *Dielectric function representation by B-splines.* physica status solidi (a), 2008. **205**(4): p. 715-719.
184. Bruggeman, D.A.G., *Berechnung verschiedener physikalischer Konstanten von heterogenen Substanzen. I. Dielektrizitätskonstanten und Leitfähigkeiten der Mischkörper aus isotropen Substanzen.* Annalen der Physik, 1935. **416**(7): p. 636-664.
185. Østreng, E., K.B. Gandrud, O. Nilsen and H. Fjellvåg, *High power nanostuctured V_2O_5 thin film cathodes made by Atomic Layer Deposition.* J. Mater. Chem. A, 2014. **Submitted**.
186. Maeng, W.J., I. Jung and J.Y. Son, *Enhanced ferroelectric polarization in tetragonally strained NaNbO3 thin film on single crystal Rh substrate.* J. Cryst. Growth, 2012. **349**(1): p. 24-26.
187. *Atomic Layer Deposition of Nanostructured Materials*. 2012: Wiley-VCH Verlag GmbH&Co.
188. Ylilammi, M., *Monolayer thickness in atomic layer deposition.* Thin Solid Films, 1996. **279**(1-2): p. 124-130.
189. Rose, M., J. Niinisto, I. Endler, J.W. Bartha, P. Kucher, and M. Ritala, *In Situ Reaction Mechanism Studies on Ozone-Based Atomic Layer Deposition of Al_2O_3 and HfO_2.* ACS Appl. Mater. Interfaces, 2010. **2**(2): p. 347-350.
190. Elliott, S.D., G. Scarel, C. Wiemer, M. Fanciulli and G. Pavia, *Ozone-Based Atomic Layer Deposition of Alumina from TMA: Growth, Morphology, and Reaction Mechanism.* Chem. Mater., 2006. **18**(16): p. 3764-3773.
191. Elliott, S.D., *Atomic-scale simulation of ALD chemistry.* Semicond. Sci. Technol., 2012. **27**(7): p. 074008/1-074008/10.
192. Knapas, K. and M. Ritala, *In Situ Studies on Reaction Mechanisms in Atomic Layer Deposition.* Crit. Rev. Solid State Mater. Sci., 2013. **38**(3): p. 167-202.

I

II

III

IV

V

VI

VII